



Article

Intra-Annual Cumulative Effects and Mechanisms of Climatic Factors on Global Vegetation Biomes' Growth

Guoming Du ¹, Shouhong Yan ^{1,2}, Hang Chen ³, Jian Yang ^{2,4} and Youyue Wen ^{2,4,*}

¹ School of Geography and Planning, Sun Yat-sen University, Guangzhou 510275, China; eesdgm@mail.sysu.edu.cn (G.D.); yanshh6@mail2.sysu.edu.cn (S.Y.)

² South China Institute of Environmental Science, Ministry of Ecology and Environment, Guangzhou 510535, China; yangjian@scies.org

³ Guangzhou Planning and Natural Resources Automation Center, Guangzhou 510055, China; chenhang@gz.gov.cn

⁴ National Key Laboratory of Urban Ecological Environment Simulation and Protection, Guangzhou 510535, China

* Correspondence: wenyoyue@scies.org; Tel.: +86-180-2241-8972

Abstract: Previous studies have shown that climate change has significant cumulative effects on vegetation growth. However, there remains a gap in understanding the characteristics of cumulative climatic effects on different vegetation types and the underlying driving mechanisms. In this study, using the normalized difference vegetation index data from 1982 to 2015, along with accumulated temperature, precipitation, and solar radiation data, we quantitatively investigated the intra-annual cumulative effects of climatic factors on global vegetation biomes across climatic zones. We also explored the underlying driving mechanisms. The results indicate that precipitation has a longer intra-annual cumulative effect on vegetation, with effects lasting up to 12 months for large percentages of most vegetation biomes. The cumulative effect of solar radiation is mostly concentrated within 0–6 months. Temperature has a shorter cumulative effect, with no significant cumulative effect of temperature on large percentages of tree-type vegetation. Compared to other vegetation types, evergreen broadleaf forests, close shrublands, open shrublands, savannas, and woody savannas exhibit more complex cumulative climatic effects. Each vegetation type shows a weak-to-moderate correlation with accumulated precipitation while exhibiting strong-to-extremely-strong positive correlations with accumulated temperature and accumulated solar radiation. The climate-induced regulations of water, heat, and nutrient, as well as the intrinsic mechanisms of vegetation's tolerance, resistance, and adaptation to climate change, account for the significant heterogeneity of cumulative climatic effects across vegetation biomes in different climatic zones. This study contributes to enriching the theoretical understanding of the relationship between vegetation growth and climate change. It also offers crucial theoretical support for developing climate change adaptation strategies and improving future "vegetation-climate" models.

Keywords: cumulative effects; NDVI; vegetation biomes; temperature; precipitation; solar radiation



Citation: Du, G.; Yan, S.; Chen, H.; Yang, J.; Wen, Y. Intra-Annual Cumulative Effects and Mechanisms of Climatic Factors on Global Vegetation Biomes' Growth. *Remote Sens.* **2024**, *16*, 779. <https://doi.org/10.3390/rs16050779>

Academic Editors: Liming Zhou, Mou Leong Tan, Cheng Li, Fei Zhang and Kwok Pan Chun

Received: 22 December 2023

Revised: 3 February 2024

Accepted: 21 February 2024

Published: 23 February 2024



Copyright: © 2024 by the authors. Licensee MDPI, Basel, Switzerland. This article is an open access article distributed under the terms and conditions of the Creative Commons Attribution (CC BY) license (<https://creativecommons.org/licenses/by/4.0/>).

1. Introduction

Climate change poses one of the greatest challenges to humanity, with intricate mechanisms and far-reaching impacts. As a vital nexus between the soil, atmosphere, and water, green vegetation serves as a sensitive barometer of climate change's effects on terrestrial ecosystems. Through photosynthesis, green vegetation absorbs atmospheric carbon dioxide and sequesters it in biomass and the soil, while releasing oxygen. This process is critical for achieving carbon neutrality in land ecosystems and will be pivotal in humanity's efforts to mitigate global climate change.

Extensive research has examined climate change's impacts on vegetation growth. For example, studies have shown that warming induces earlier onset and extended duration

of the growing season, altering vegetation's phenological traits. Additionally, warming enables the expansion of habitats suitable for vegetation growth towards higher latitudes and elevations [1–3]. Warming can also boost vegetation's carbon sequestration capacity [4,5]. However, increases in extreme weather like heatwaves and droughts can indirectly constrain vegetation growth, transforming some carbon sinks into sources [6–8].

Climate change is typified by fluctuations in factors like temperature, solar radiation, and precipitation—the three most widely used climatic indices [4,9,10]. These factors shape plant growth and distribution by influencing processes including photosynthesis, respiration, and soil carbon decomposition. As key determinants of vegetation growth, temperature enhances productivity in colder regions [4,11], while solar radiation is the prime driver of tropical rainforest productivity [4,8,12]. In arid areas, precipitation most strongly governs vegetation productivity changes [13,14]. These factors are critical and frequently used to characterize vegetation growth shifts. Research suggests that over half of vegetation change can be attributed to variations in these three factors [4,9].

Climate change does not immediately impact vegetation. Instead, a noticeable time-lag exists. For instance, vegetation growth at middle and low latitudes exhibits a 1–3 month lag in responding to temperature changes, while middle- and high-latitude areas show a 1–3 month lag in responding to solar radiation [15]. Precipitation also induces a 1 month lag in arid and semi-arid regions [15]. Across China, a 0–1 month lag is typical in vegetation responses to temperature and precipitation changes [16]. In the Amazon basin, lags of 0–6 months (temperature), 0–9 months (radiation), and 0–6 months (precipitation) have been observed [17]. At the global scale, radiation, soil moisture, and temperature drive 0–3 month lags in vegetation growth [18]. These studies indicate that historical climatic conditions often have the strongest impact on current growth. This lag provides vegetation time to respond to changes, preventing drastic effects from abrupt anomalies.

The lag duration is primarily determined by changes in vegetation water content [19]. The timing of nutrient and water storage, transport, and excretion within the vegetation also play a role [20]. In addition, the long-term balancing and synergistic mechanisms between vegetation growth and environmental factors like soil moisture and carbon/nitrogen [21–23], along with intrinsic mechanisms conferring climate resilience like drought tolerance [24] and the thermal adaptation of photosynthesis/respiration [25–27], are also important driving factors behind the lagged effects.

Furthermore, recent research shows that climate change has a long-term, cumulative impact on vegetation growth [28]. This cumulative effect is widely observed across climates. For instance, temperature has a negligible cumulative effect in most of the Arctic and Northern Temperate Zones but a substantial 2–3 months effect in arid/semi-arid areas. Solar radiation induces a noticeable 3-month cumulative effect in the Arctic and Northern Temperate Zones, while it is shorter in other regions. Precipitation shows complex spatial cumulative effects. This research highlights the prolonged, compounding nature of climate change impacts on vegetation growth and indicates that considering the cumulative effect of climate, the relationship between “climate change-vegetation growth” can be better characterized. On a global scale, the average fitting capability is improved by 12.94%, with a maximum improvement of up to 76.85%. The fitting capability of climatic factors to vegetation growth can be effectively enhanced in approximately 77% of vegetation regions globally, especially in regions with strong interaction between vegetation and climatic factors, such as arid and semi-arid areas. These research findings have been widely confirmed by subsequent studies.

Based on the concept of cumulative effects [28], many scholars have further revealed that the intensity of cumulative climatic effects on vegetation growth varies over different growing seasons [29–34]. Specifically, a study conducted in Siberia [29] found that climatic factors exhibit an average cumulative effect of 3.6 months on vegetation growth throughout the entire growing season, with more complex ecosystems showing longer cumulative effects. In a study conducted in Inner Mongolia [35], it was discovered that temperature and precipitation have a cumulative effect on vegetation growth for up to two months, but

the contribution of climatic factors to the current vegetation growth varies depending on the month, with the highest contribution coming from the current month. It has been found that cumulative drought effects impact the photosynthesis process of 52.11% of global vegetation, with an average cumulative duration of 1–4 months [32]. Furthermore, more than three-quarters (78.55%) of grasslands globally are affected by cumulative drought effects, lasting 8–10 months in arid regions of the northern hemisphere (40°N–55°N) [31] and 5–10 months in the Qinghai–Tibet Plateau region of China [34]. Meanwhile, some researchers have attempted to couple cumulative climatic effects into the “climate change–vegetation growth” relationship model in order to better characterize the response of vegetation growth to climate change [30,33,35].

Based on previous research, it can be summarized that climate change has significant cumulative effects on vegetation growth, exhibiting heterogeneity across different climate regions and vegetation types. However, the existing studies mentioned before did not systematically disentangle the effects of cumulative climatic effects on different vegetation types at global scale, and the underlying driving mechanisms remain poorly understood. Specifically, as climatic conditions transition throughout the year, vegetation growth undergoes a distinct cyclic pattern of changes, these studies have not effectively captured the crucial intra-annual impacts of climatic variability on vegetation growth cycles, which hinders a comprehensive understanding of the relationship between climate change and vegetation growth. Therefore, this study utilized the satellite-derived Normalized Difference Vegetation Index (NDVI) and corresponding climate data (temperature, precipitation, solar radiation) from 1982 to 2015 to investigate the differential responses of major global vegetation types in different climatic zones to the cumulative effects of climatic factors. The present study also attempted to unravel the underlying driving mechanisms. Specifically, this study first extracted the spatial distribution of unchanged vegetation types during the study period. Then, through partial correlation and time-lag analyses, we examined the magnitude and duration of the cumulative effects of temperature, precipitation, and radiation on vegetation growth in these unchanged regions. We analyzed how these effects differ across vegetation types and climatic zones. Finally, we explored the potential mechanisms driving the observed cumulative climatic effects. Overall, this study provides new insights into differential vegetation responses to cumulative climatic effects over time. Our findings bridge knowledge gaps regarding vegetation–climate interactions and support climate-change-mitigation policies.

2. Data

2.1. NDVI Data

This study utilized the Global Inventory Monitoring and Modelling Studies Group (GIMMS)'s third generation NDVI dataset (GIMMS NDVI3g v1.0) to characterize vegetation growth conditions. The NDVI3g dataset has a spatial resolution of 8 km, has a temporal resolution of 15 days, and spans July 1981 to December 2015 for global land areas outside of Antarctica. We processed the data into monthly values using the Maximum Value Composite (MVC) method to minimize contamination from non-vegetation signals. The NDVI3g dataset provides a long time series, extensive spatial coverage, and high accuracy for monitoring and evaluating large-scale vegetation dynamics [15,36–38]. Moreover, the statistical analyses in this study were based on the vegetation growing season, which was defined as those months with monthly average air temperature > 0 °C and NDVI > 0.2 [15,39]. We used the subset of January 1982 to December 2015 in this study.

2.2. Climate Data

The climate data include monthly mean temperature (TEM), total monthly precipitation (PRE), and total monthly shortwave solar radiation (SOLAR) at 0.5° spatial resolution from January 1982 to December 2015. TEM and PRE are from the Climatic Research Unit (CRU) Time-Series Version 3.24 dataset, which incorporates additional station data and corrects known errors relative to earlier versions [40]. SOLAR is from the Princeton Global

Meteorological Forcing Dataset version 2, which implements improved downscaling and bias correction methods [41]. These datasets have been widely used in global vegetation–climate studies [15,28,36,37,42–44]. The climatic datasets were interpolated into 8 km using kriging interpolation.

2.3. Vegetation Type Data

The vegetation classification was based on the 1 km University of Maryland (UMD) land cover product derived from 14 years (1981–1994) of Advanced Very High Resolution Radiometer (AVHRR) data. It provides 14 land use/cover types with a relatively high overall classification accuracy ranging from 81.4% to 90.3% [45]. Furthermore, this study obtained the 500 m land use/cover product (MCD12Q1) from The Moderate Resolution Imaging Spectroradiometer (MODIS) satellite for the year of 2015. The UMD scheme with 11 vegetation types (Figure 1) was adopted, with non-vegetated areas masked out. Using the UMD and MCD12Q1 land use/cover data, the unchanged vegetation pixels for each vegetation biome were identified during the study period. Combined with the distribution of four climatic zones (Figure 1), we extracted the average values of NDVI and climatic factors for each vegetation biome in each climatic zone and then analyzed the climatic cumulative effects on different types of vegetation in different climatic zones. In addition, to conduct a more detailed analysis, we utilized the climatic zone data from IPCC (Figure A8) and the global distribution data of the four major crops (maize, rice, soybean, and wheat) provided by the Chinese Academy of Agricultural Sciences.

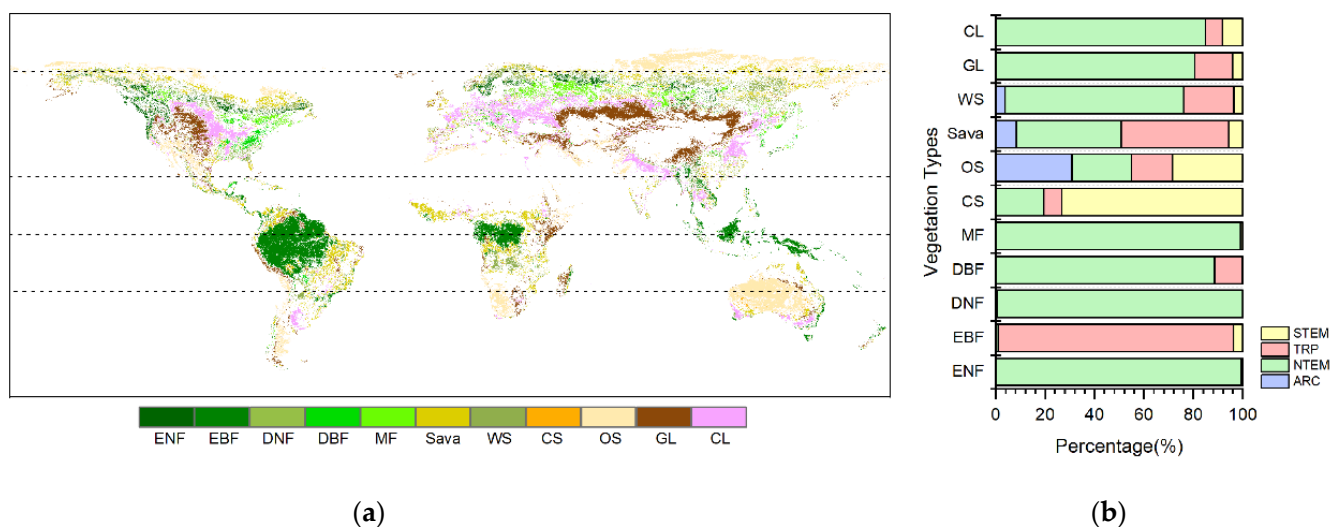


Figure 1. (a) Spatial distribution map of unchanged vegetation types worldwide from 1982 to 2015; (b) a stacked bar chart illustrating the percentage distribution of different climatic zones. Evergreen Needleleaf Forest (ENF), Evergreen Broadleaf Forest (EBF), Deciduous Needleleaf Forest (DNF), Deciduous Broadleaf Forest (DBF), Mixed Forest (MF), Closed Shrubland (CS), Open Shrubland (OS), Savannas (Sava), Woody Savannas (WS), Grassland (GL), and Cropland (CL). Four climatic zones were divided [28]: the Arctic Zone (ARC, 66.5°N–90.0°N), the Northern Temperate Zone (NTEM, 23.5°N–66.5°N), the Tropic Zone (TRP, 23.5°S–23.5°N), and the Southern Temperate Zone (STEM, 23.5°S–66.5°S).

The data processing procedure and research methods are shown in Figure 2. In the figure, the blue boxes represent data processed using ArcGIS 10.8 software, and red box represents data processed using MATLAB. Please note that, to minimize the loss of data information, the post-processed datasets were resampled to 500 m to match the spatial resolution of MCD12Q1. Our analyses focused on areas where vegetation types remained unchanged during the study period.

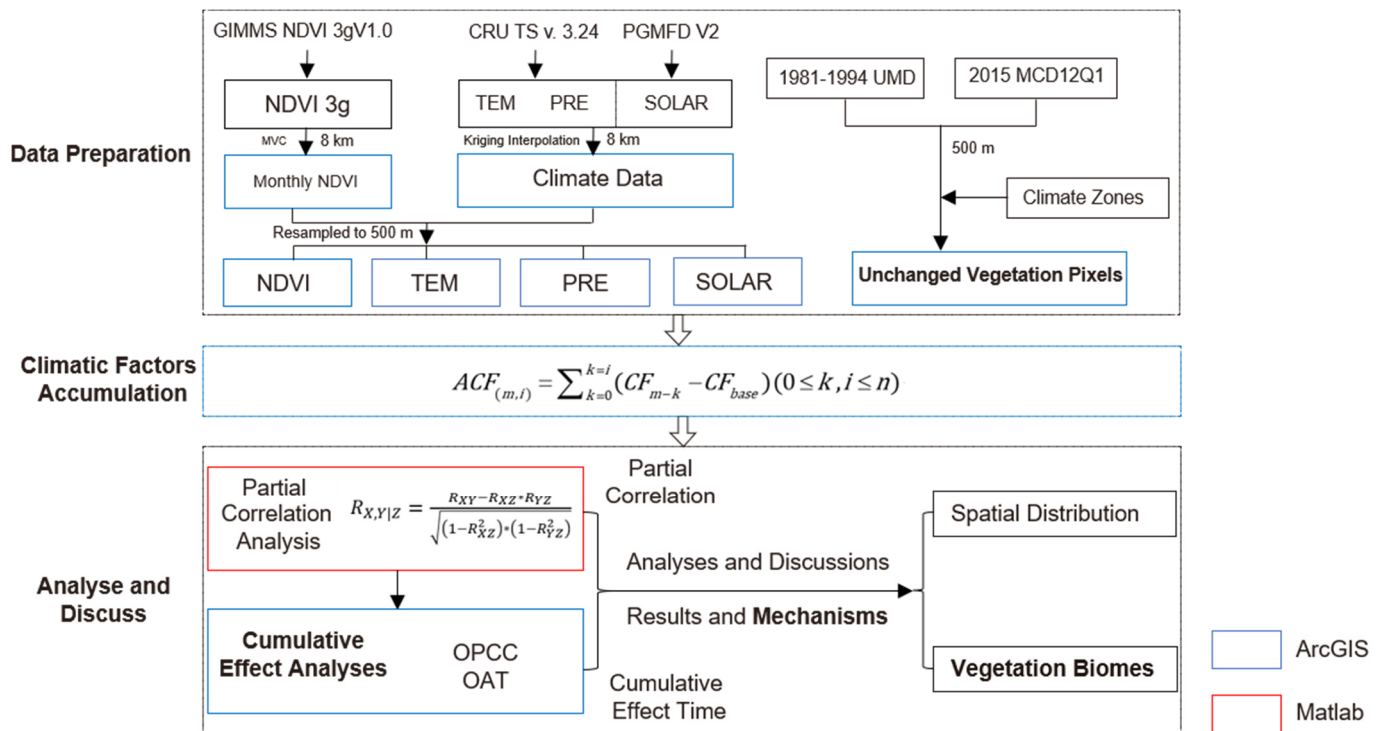


Figure 2. Technology roadmap.

3. Methods

3.1. Accumulated Climatic Factors

We defined accumulated climatic factors, including accumulated temperature (ATEM), accumulated solar radiation (ASOLAR), and accumulated precipitation (APRE), to represent the historical magnitude of climate change. These cumulative factors were calculated by summing the monthly climate data exceeding specified thresholds over a given time period, as follows:

$$ACF_{(m,i)} = \sum_{k=0}^{k=i} (CF_{m-k} - CF_{base}) (0 \leq k, i \leq n) \quad (1)$$

where ACF is the accumulated climatic factors, namely, ATEM, ASOLAR, and APRE. CF is the time series data of the original climatic factors corresponding to ACF . CF_{base} is the threshold corresponding to the cumulative climate factors. Based on previous studies, the thresholds for ATEM, ASOLAR, and APRE were set at 0°C , 0 W/m^2 , and 0 mm , respectively [28]. m is the monthly time series, ranging from January 1982 to December 2015. i is the cumulative time period. k is the difference between the current month and the cumulative months. When monthly data were below the thresholds, the cumulative values remained unchanged from the prior month. We set the maximum accumulation period (n) to 12 months, consistent with typical annual vegetation cycles [46,47].

For example, the cumulative temperature data for December 2000 with an accumulative time of 3 months was obtained by summing the temperature values for October, November, and December of 2000. If the temperature for a month was below 0°C , 0 was added instead.

3.2. Partial Correlation Analyses and Cumulative Effect Analyses

Partial correlation analysis was used to examine relationships between NDVI and one typical accumulated climatic factor while controlling others [28]. The partial correlation

coefficient takes values $[-1, 1]$, representing complete negative correlation to complete positive correlation in statistics. The calculation formula is as follows:

$$R_{X,Y|Z} = \frac{R_{XY} - R_{XZ} \times R_{YZ}}{\sqrt{(1 - R_{XZ}^2) \times (1 - R_{YZ}^2)}} \quad (2)$$

where X, Y and Z are the independent variable, dependent variable, and control variable, respectively. $R_{X,Y|Z}$ represents the partial correlation coefficient between X and Y after removing the influence of the Z variable. R_{XY} , R_{XZ} , and R_{YZ} are the Pearson correlation coefficients between X and Y , X and Z , and Y and Z , respectively. When the absolute value of the partial correlation coefficient is between 0.8 and 1.0, it indicates a very strong correlation. A correlation between 0.6 and 0.8 is considered strong, 0.4 to 0.6 indicates a moderate degree of correlation, 0.2 to 0.4 suggests a weak correlation, and 0.0 to 0.2 indicates a very weak correlation or no correlation.

In this study, the accumulated duration ranges from 0 to 12 months. For each assumed accumulated duration, a partial correlation coefficient can be calculated. When a partial correlation coefficient reaches the maximum coefficient of determination, the corresponding accumulated duration is considered the optimal accumulated time (OAT). The partial correlation coefficient at this duration is also considered the optimal partial correlation coefficient (OPCC). The specific formula is as follows:

$$OPCC = PCC_k, \text{ when } PCC_k^2 = \text{Maximum} \{ PCC_0^2, PCC_1^2, \dots, PCC_i^2, \dots, PCC_{12}^2 \} (0 \leq k, i \leq 12) \quad (3)$$

$$OAT = k, \text{ when } PCC_k^2 = \text{Maximum} \{ PCC_0^2, PCC_1^2, \dots, PCC_i^2, \dots, PCC_{12}^2 \} (0 \leq k, i \leq 12) \quad (4)$$

where $OPCC$ is the optimal partial correlation coefficient. i is the assumed accumulated duration, with values ranging from 0 to 12. k is the cumulative duration associated with the maximum deterministic coefficient. PCC_k is the partial correlation coefficient at a certain assumed cumulative duration. PCC_k^2 is the coefficient of determination for that correlation coefficient. OAT is the optimal accumulated time.

For example, we first calculate the partial correlation coefficients between the NDVI of a certain pixel and 13 cumulative temperature time series data from 0 to 12 months, with the corresponding cumulative precipitation and cumulative solar radiation data as control variables. The cumulative time corresponding to the largest squared value of these 13 partial correlation coefficients is the optimal cumulative time for the temperature of this pixel.

4. Results

4.1. Global Distribution of Unchanged Vegetation Types

According to Figure 1, it can be observed that the unchanged vegetation types were widely distributed in the northern temperate (NTEM) and tropical (TRP) climatic zones during the study period. Most of the ENFs, DNFs, DBFs, MFs, WS, GLs, and CLs were located in NTEM, accounting for 99.20%, 99.13%, 88.65%, 99.10%, 72.40%, 80.32%, and 84.94%, respectively. EBFs were predominantly in the TRP at 95.24%. CS were mainly in the southern temperate (STEM) zone at 73.31%. OSs were more evenly distributed across climatic zones. Sava were mostly found in NTEM and TRP (85.94% combined).

Comparing with the global climate regions defined by the Intergovernmental Panel on Climate Change (IPCC), the following were found (Figure 3): ENFs are mainly distributed in the Cool Temperate Moist (42%) and Boreal Moist (48%) climate regions. EBFs are primarily found in the Tropical Wet (60%) and Tropical Moist (32%) climate regions. DNFs are mainly in the Boreal Moist (64%) and Boreal Dry (36%) climate regions. DBFs are primarily in the Cool Temperate Moist (42%), Warm Temperate Moist (39%), and Tropical Moist (10%) climate regions. MFs are predominantly located in the Cool Temperate Moist (67%) and Boreal Moist (25%) climate regions. CSs are largely distributed in the Tropical

Dry (69%) and Warm Temperate Dry (10%) zones. OS are mostly in the Tropical Dry (38%), Polar Moist (19%), Boreal Moist (18%), and Warm Temperate Dry (13%) climate regions. Sava are mainly distributed in the Tropical Moist (30%) and Boreal Moist (28%) climate regions. WS are mostly located in the Boreal Moist (40%), Cool Temperate Moist (13%), and Tropical Moist (10%) climate regions. GLs are primarily found in the Cool Temperate Dry (50%) and Warm Temperate Dry (13%) climate regions. CLs are mainly distributed in the Cool Temperate Dry (30%), Warm Temperate Dry (25%), and Cool Temperate Moist (21%) climate regions.

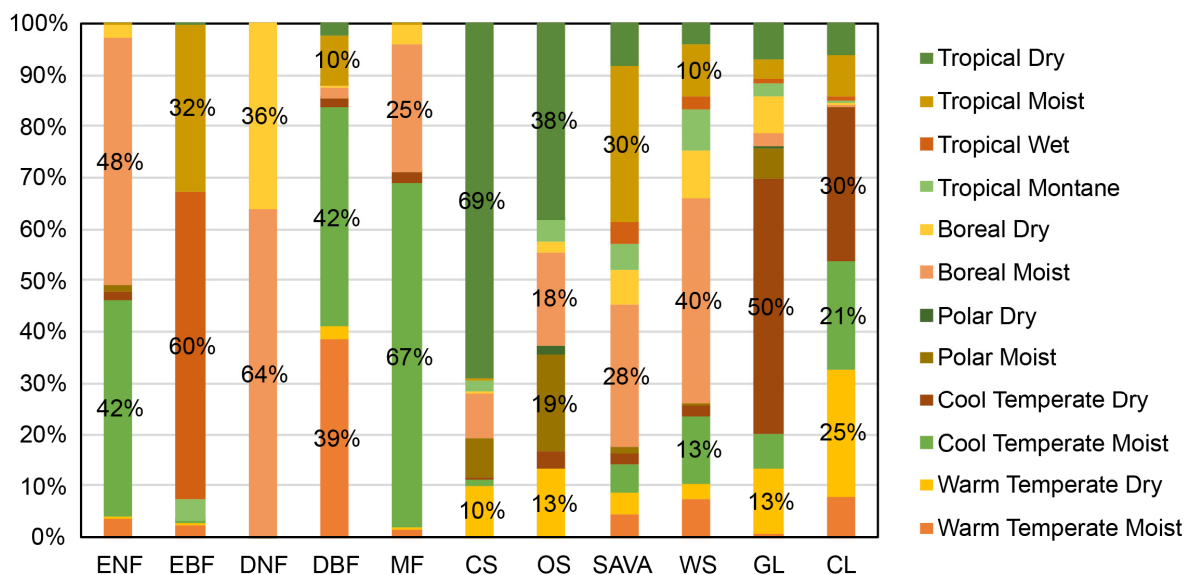


Figure 3. Distribution proportion of different types of vegetation in dry and wet climate zones. Here, the climate zones were defined by IPCC (<https://esdac.jrc.ec.europa.eu/projects/RenewableEnergy/>, accessed on 2 September 2023).

4.2. Accumulated Climatic Effect Durations

The cumulative effects of precipitation on vegetation growth showed complex patterns across climatic zones and vegetation types (Figures 4 and 5). Different optimal accumulation durations were observed, varying significantly by region and vegetation type. Globally, ENFs exhibited cumulative precipitation effects mainly at 6–7 months (31.15%) and 12 months (32.79%). EBFs responded primarily at 0–3 months (40.49%). DNFs showed a major response at 2–3 months (58.07%). DBF effects accumulated over 12 months (43.33%) and 0–3 months (31.55%). MFs were mainly distributed in NTEM, and 59.00% of MFs in this climate zone exhibited a cumulative response to precipitation for up to 12 months, resulting in a 12-month cumulative effect on 58.59% of global MF growth. CSs in NTEM accumulated effects over 7–12 months (78.71%) versus 3–10 months in STEM (94.32%), showing a mixed global pattern. OSs, Sava, and WS demonstrated similar heterogeneity as CSs. However, it is worth noting that for Sava and WS in NTEM, 12-month effects were notable at 30.36% and 22.28%. GLs and CLs exhibited primary global responses at 12 months (38.62% and 40.52%) and 0–3 months (41.35% and 32.52%).

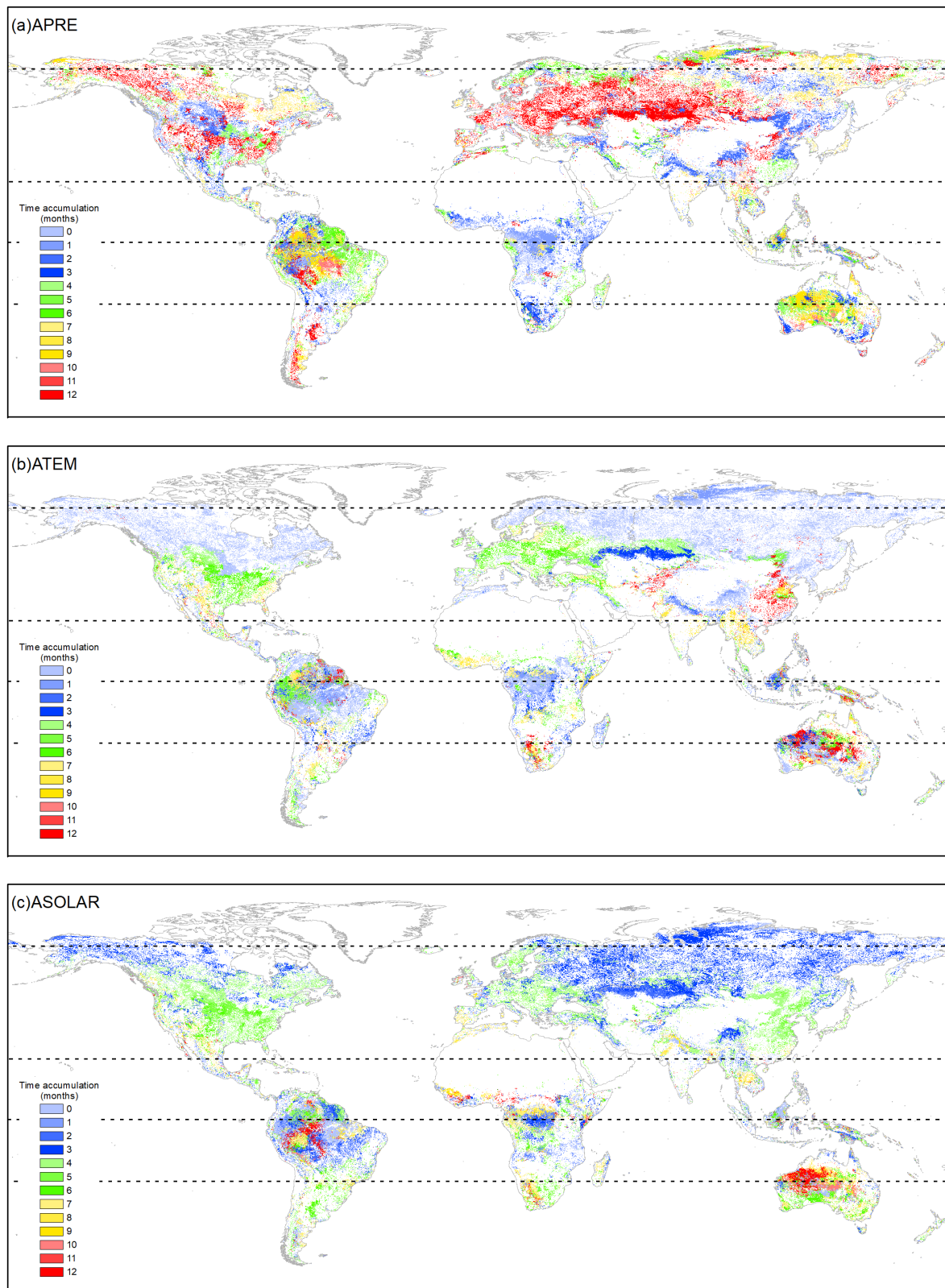


Figure 4. The distribution of accumulation effects durations of climatic factors (a) APRE, (b) ATEM, and (c) ASOLAR on vegetation growth from 1982 to 2015. The white areas represent regions with a p -value greater than 0.05, areas with vegetation type transitions, or non-vegetated areas.

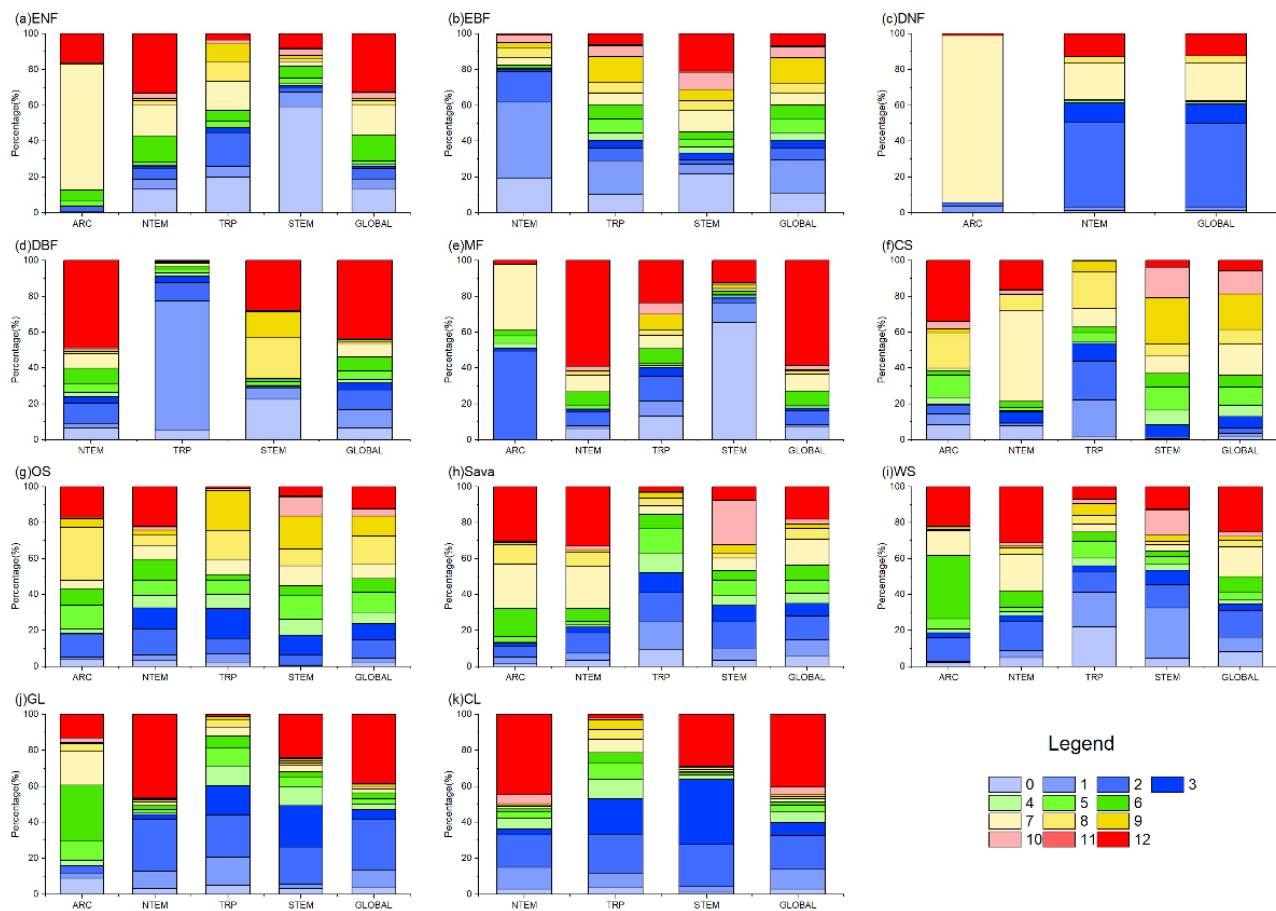


Figure 5. The proportion of OAT of PRE on global vegetation biomes. In the figure, (a) ENF, (b) EBF, (c) DNF, (d) DBF, (e) MF, (f) CS, (g) OS, (h) Sava, (i) WS, (j) GL, and (k) CL are shown.

According to Figures 4 and 6, the cumulative effects of solar radiation on vegetation growth were mainly concentrated within 0–6 months across climate zones and vegetation types. However, some differences existed in the dominant response durations. Globally, ENFs showed primary cumulative solar effects within 3–4 months (70.42%), driven by the response in NTEM. EBFs exhibited a 0–3-month response (57.55%) worldwide, with balanced effects in other months. Over 97% of global DNFs responded within 1 month consistently across all climatic zones. Regarding DBFs, NTEM exhibited cumulative solar effects accumulated over 3–5 months (93.36%), versus 1–2 months (48.32%) and 5–6 months (29.83%) in TRP, and 6–7 months (84.08%) in STEM. Considering all zones, the global cumulative effects of solar radiation on DBF mainly occurred within 3–5 months (84.31%). MFs responded predominantly within 3–4 months (91.69%). CS showed shorter cumulative solar effects in NTEM (0–4 months, 96.13%) than in STEM (4–7 months, 60.41%; 10–12 months, 24.80%). The cumulative effects of solar radiation on OS, Sava, WS, and GLs shared similar characteristics with CSs. However, unlike CSs, a significant proportion of OSs (31.39%) exhibited a response to accumulated solar radiation for up to 12 months in TRP, and a considerable proportion of GLs (41.18%) showed an instantaneous response in ARC. At a global scale, solar radiation had a dominant cumulative effect on CLs within 3–6 months (79.55%).

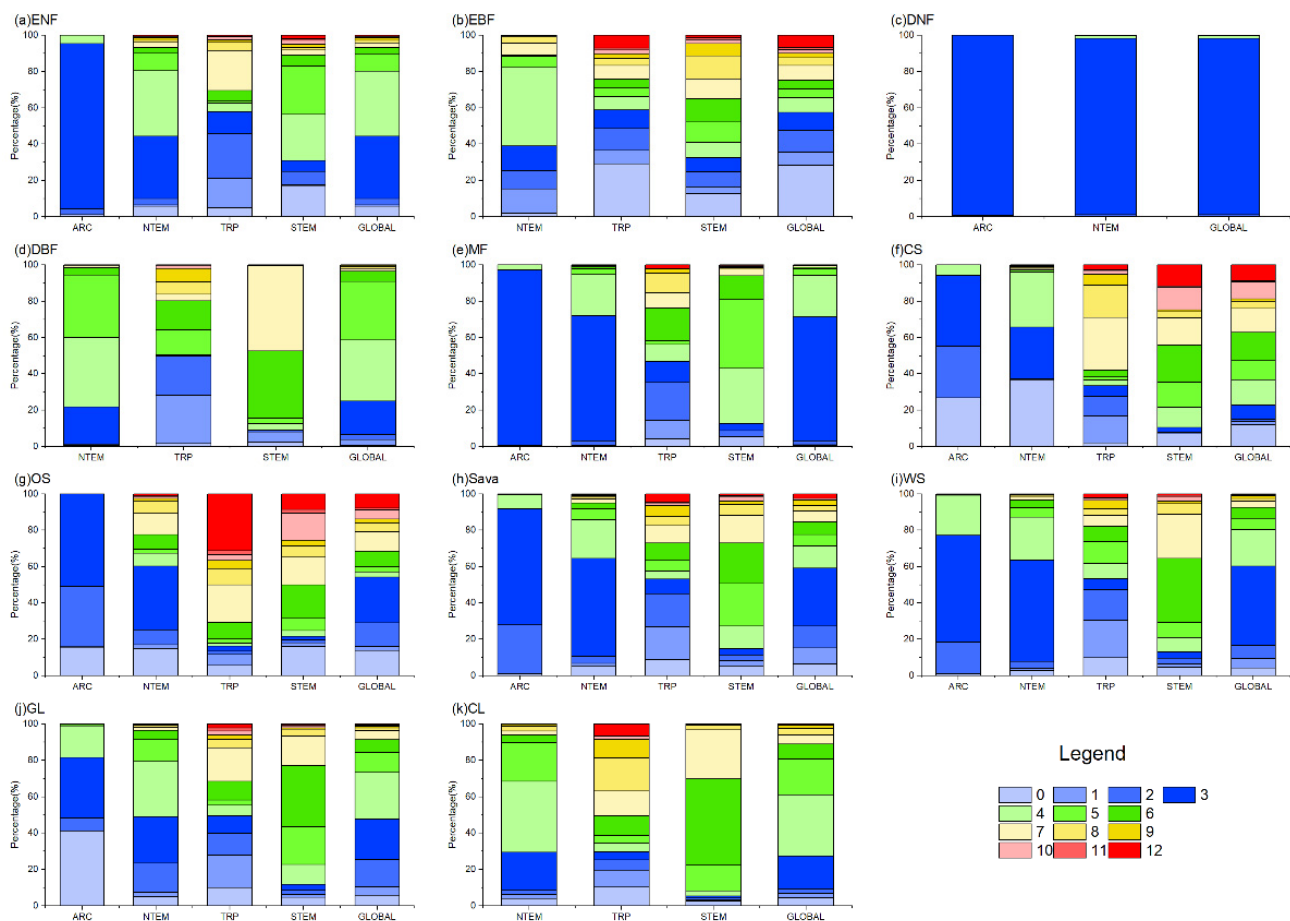


Figure 6. The proportion of OAT of SOLAR on different vegetation types globally. In the figure, (a) ENF, (b) EBF, (c) DNF, (d) DBF, (e) MF, (f) CS, (g) OS, (h) Sava, (i) WS, (j) GL, and (k) CL are shown.

Figures 4 and 7 show that in ARC, the cumulative temperature effect on almost all vegetation types was within 0–1 month, indicating an urgent temperature requirement for vegetation growth in these regions. In NTEM, a large portion of ENFs (80.38%), DNFs (98.63%), MFs (87.09%), CSs (80.71%), Sava (76.64%), and WS (79.58%) exhibited a cumulative temperature response of 0 months. EBFs (67.65%) responded predominantly over 8–9 months, while DBFs showed 0 months (39.86%) and 6–7 months (54.87%). GL (87.41%) and CLs (85.94%) responded mostly within 0–6 months. In TRP, the cumulative effect of temperature on vegetation biomes was more complex, with no clear dominance. However, ENFs, MFs, and OSs showed notable 12-month responses compared to other zones. In STEM, there were significant cumulative temperature effects of 5–7 months for ENFs (56.85%), 1–2 months for DBFs (81.17%), and 6–7 months for MFs (65.36%). CSs and OSs both demonstrated 0-month (37.18%, 30.83%) and 12-month (21.96%, 21.52%) effects. CLs showed 0-month (44.36%) and 7-month (28.17%) effects. Other types had relatively even temperature responses.

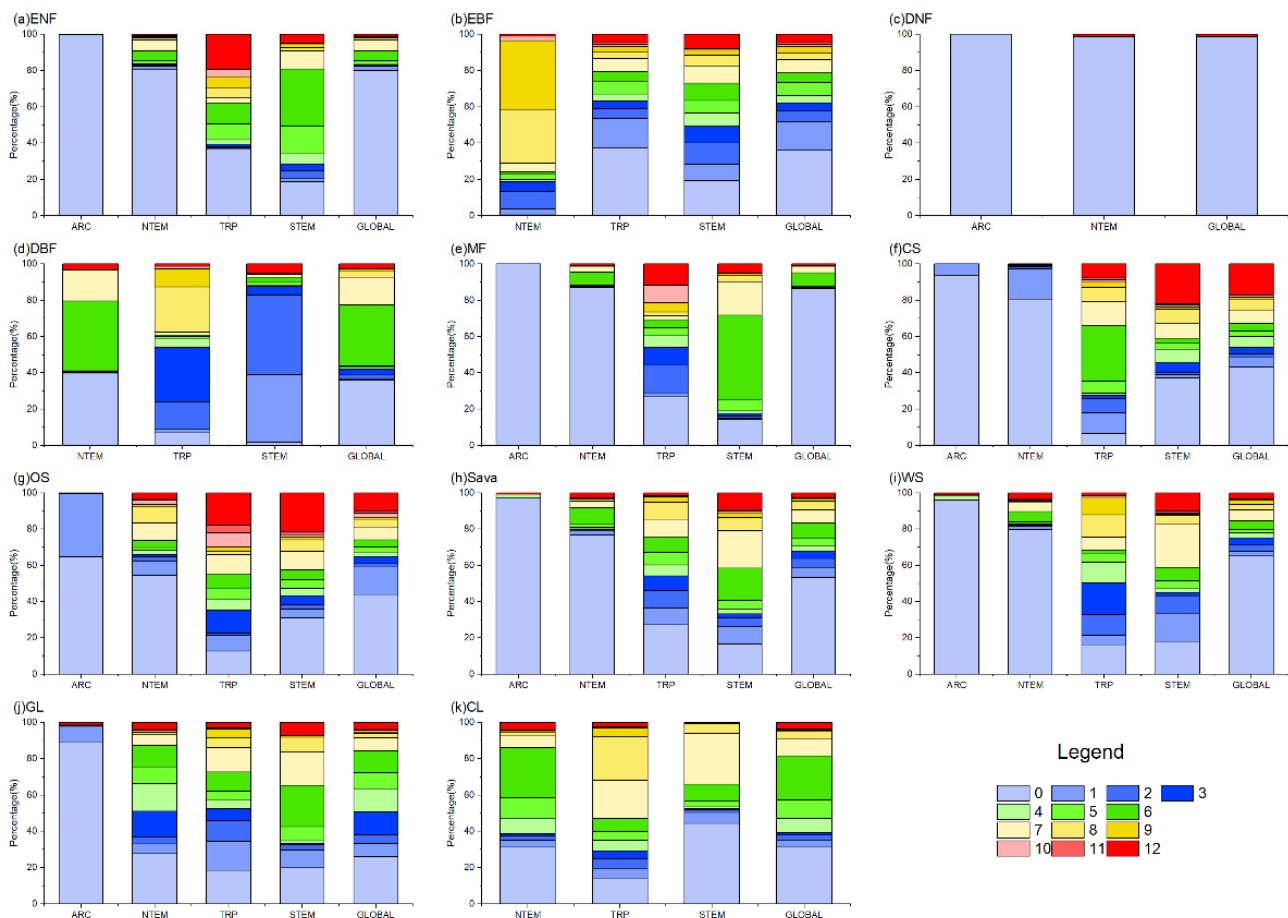


Figure 7. The proportion of OAT of TEM on different vegetation types globally. In the figure, (a) ENF, (b) EBF, (c) DNF, (d) DBF, (e) MF, (f) CS, (g) OS, (h) Sava, (i) WS, (j) GL, and (k) CL are shown.

4.3. Correlations between Accumulated Climatic Factors and Vegetation Growth

Regarding APRE correlation (Figures A1 and 8), vegetation types generally exhibited a weak correlation. In ARC, on average, over 70% of pixels for each vegetation type showed a weak or very weak negative correlation, especially ENFs, DNFs, and GLs (81.41%, 93.02%, 88.52%). For MFs, 52.52% of the pixels showed a weak positive correlation. In NTEM and STEM, over 75% of the pixels for DNFs, DBFs, OSs, Sava, WS, GLs, and CLs were primarily weakly positively correlated. Notably, OSs and GLs had a significant proportion of pixels showing a strong positive correlation in STEM (averaging around 15%). ENFs was mainly weakly correlated in NTEM (43.71% positive, 54.11% negative), but weakly negatively correlated in STEM (76.84%). EBFs exhibited a weak or very weak negative correlation in NTEM (73.05%) but a weak or very weak positive correlation (72.94%) in STEM. The situation was reversed for MFs compared to EBFs. CSs was weakly negatively correlated in NTEM (75.90%) but moderately, strongly positively correlated in STEM (86.21%). In TRP, there was a relatively strong correlation between APRE and vegetation growth. Specifically, on average, around 65% of the pixels for each vegetation type exhibited a weak-to-moderate positive correlation. CSs, OSs, Sava, WS, GLs, and CLs had significant strong positive proportions (67.63%, 23.82%, 21.57%, 32.85%, 23.57%, respectively).

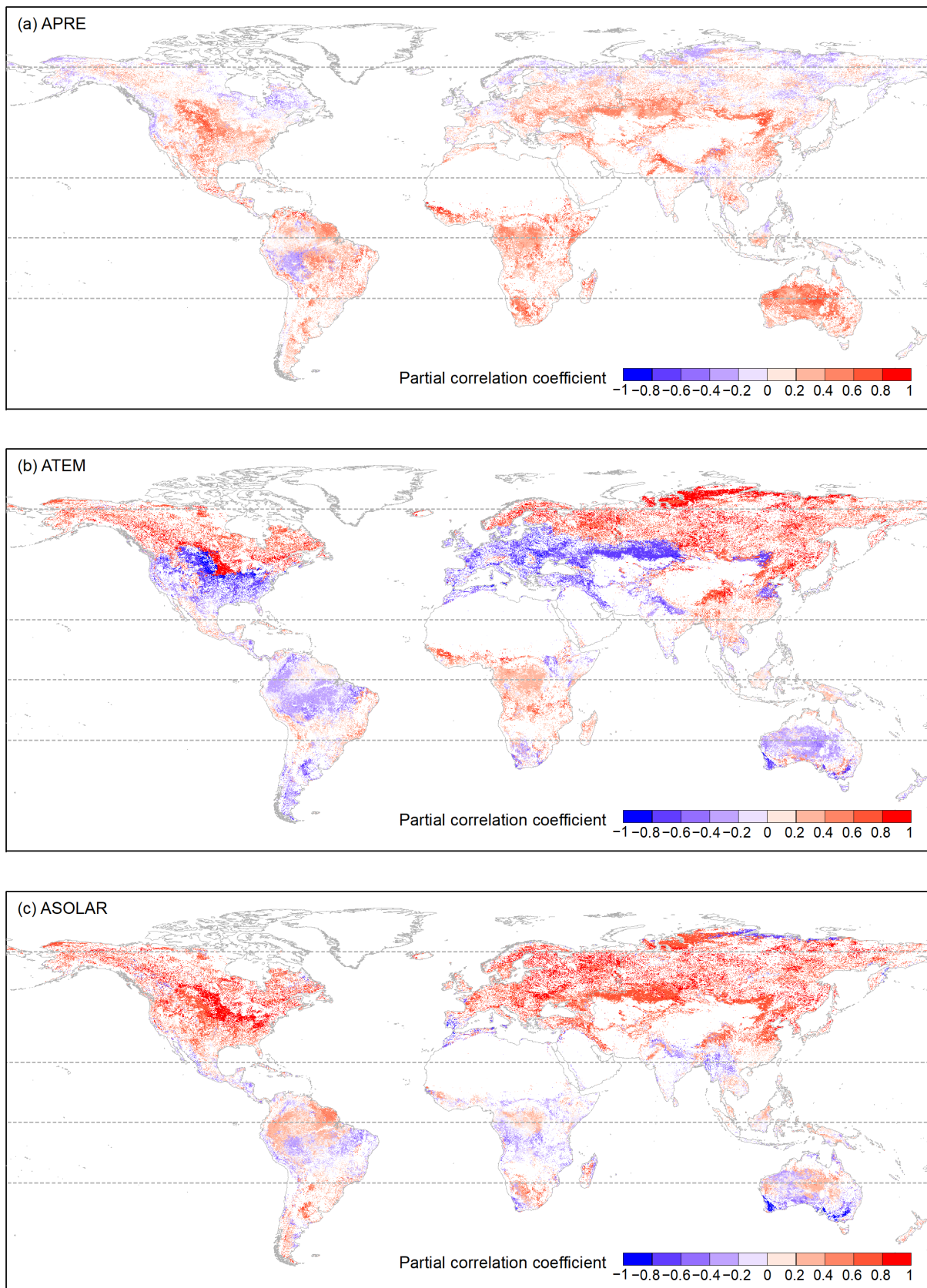


Figure 8. The distribution of OPCC between global vegetation growth and accumulated climate factors (a) APRE, (b) ATEM, and (c) ASOLAR from 1982 to 2015. The white areas represent regions with a p -value greater than 0.05, areas with vegetation type transitions, or bare areas.

For the ASOLAR correlation (Figures A2 and 8), vegetation types showed significant heterogeneity across climate zones. In ARC, all vegetation biomes exhibited strong to very strong positive correlations (>98% for ENFs, DNFs, MFs, Sava, WS). In NTEM, over 90% of DNFs, DBFs, MFs, WS, and CLs showed strong to very strong positive correlations. ENF, Sava, and GL showed moderate and above-positive correlations (~90%). A total of 86.82% of EBFs exhibited weak-to-strong negative correlations, while CSs correlated strongly positively (53.19%) and negatively (24.08%). In TRP, all vegetation types showed weak or lower correlations with roughly equal positive/negative proportions. In STEM, the correlation patterns were more complex. ENFs, DBFs, and MFs had weakly strongly positive correlations (77.79%, 90.48%, 87.51%), while over half of EBFs and WS had a weakly moderately positive correlation (58.42%, 55.42%). A total of 48.62% of CSs exhibited a weak-to-moderate negative correlation. A total of 81.63% of OSs displayed a weak or lower correlation (with positive correlation accounting for 49.69%). Sava and WS showed predominantly weak-to-moderate correlations (79.60% 78.85%) with positive proportions of 43.12% and 55.42%, respectively. A total of 64.61% of GLs exhibited moderate-to-strong positive correlations, while 51.89% of CLs showed strong and above-negative correlations. Lastly, 38.20% of CLs also exhibited moderate-to-strong positive correlations.

Regarding the correlation with ATEM (Figures A3 and 8), vegetation types differed significantly in strength. In ARC, most ENFs, DNFs, MFs, CSs, OSs, Sava, WS, and GLs exhibited strong-to-very strong positive correlations (>95% pixels). In NTEM, the majority of ENFs, DNFs, MFs, CSs, Sava, and WS showed strong-to-very strong positive correlations (>72%). In TRP, most vegetation biomes displayed weak or lower correlations. In STEM, 80.44% of ENFs showed negative weak-to-strong correlations, and 78.75% of EBF exhibited a weak or lower correlation. A total of 89.78% of DBF showed weak-to-moderate positive correlations. A total of 79.92% of MF showed moderate-to-strong negative correlations. A total of 70.04% of CS exhibited weak-to-moderate negative correlations, a total of 83.03% of OS showed moderate and below-negative correlations. Sava and WS exhibited weak-to-moderate correlations (80.65%, 78.55%) with positive and negative areas being roughly equal. A total of 78.98% of GL exhibited moderate-to-strong correlations (with negative correlations accounting for 47.06%), and 75.43% of CL showed negative moderate-to-strong correlations.

5. Discussion

This study found that a large proportion of ENFs, MFs, and DBFs had a cumulative effect on precipitation for up to 12 months (weakly positive correlation). These vegetation types are mainly distributed in the Cool Temperate Moist and Boreal Moist climate regions, accounting for over 85% of the total. This may be due to the deep root systems of these vegetation types, which allow them to effectively utilize moisture from the deeper soil layers to sustain growth while reducing dependency on current precipitation. However, the long-term accumulation of precipitation replenishes moisture in deeper soils, promoting the growth of these forests [48]. Additionally, the complex ecosystem composition of MFs leads to niche partitioning and growth-promotion mechanisms. MFs exhibit strong adaptation mechanisms, including tolerance, avoidance, and recovery, to cope with drought [49–52]. The higher evapotranspiration, lower ecological connectivity, and increased water demand during the growing season in DBFs likely contributes to its long-term cumulative precipitation effect [48,53,54]. DNFs show a shorter cumulative effect of precipitation compared to DBFs, consistent with previous findings [15,48]. The study also indicates that a significant proportion of DNF pixels exhibit a short response (2 months) to APRE, mainly in the Boreal Moist climate, suggesting a significant and urgent demand for precipitation by DNFs in this climate zone. EBFs primarily grow in hot and humid tropical and subtropical regions. This study found that EBFs in these two regions mainly exhibited weak or very weak negative correlations with APRE, potentially due to increased evapotranspiration, reduced radiation, and unfavorable temperatures for EBFs' growth [15].

GANG C et al. [55] found that the NPP of GLs is positively correlated with annual mean precipitation, while its correlation with annual average temperature varies. This aligns with the current study's findings. The regions with a high GL distribution in NTEM, TRP, and STEM all showed a positive correlation of over 90% with APRE and a varying proportion of positive and negative correlations with ATEM. GLs are mainly distributed in the Cool Temperate Dry climate regions of North America and Eurasia in NTEM, and the Qinghai–Tibet Plateau (Cool Temperate Moist climate region). In the Cool Temperate Dry regions, limited water resources due to scarce precipitation and high evapotranspiration become the most important growth-limiting factors, resulting in a moderate positive correlation between grassland and precipitation in NTEM as found by this study. The shallow root systems of GLs enable a quick response to alleviated water limitations from precipitation inputs. Due to the urgent precipitation demand, any rainfall during a growing season significantly promotes growth [56,57]. Therefore, previous research [15] discovered a short lag effect (1 month) of precipitation on GLs, while this study found a longer cumulative effect of precipitation (12 months). On the other hand, GLs in the Qinghai–Tibet Plateau (Cool Temperate Moist climate region) can mitigate water limitations through snow-cover melting. As a result, the demand for precipitation by GLs is not strong, leading to a significantly smaller cumulative effect of precipitation (3 months). CLs are primarily distributed in the Cool Temperate Dry, Cool Temperate Moist, and Warm Temperate Dry climate regions. In these areas, approximately half of the CLs exhibited a cumulative effect of precipitation lasting up to 12 months, indicating a long-term influence of precipitation.

Vegetation growing in high-latitude and high-altitude regions is primarily temperature-dependent [15]. Temperature influences vegetation growth by increasing photosynthetic enzyme activity [58] and reducing autumn foliage degradation rates [59], promoting vegetation growth. This rapid response [15,48] has led to urgent temperature response mechanisms in these vegetation types. This may be an important reason for the strong positive temperature correlation and short cumulative temperature effects (0–1 month) for Cool Temperate climate vegetation types such as ENFs, DNFs, DBFs, MFs, WS, Sava, and, specifically, GLs on the Qinghai–Tibet Plateau. Furthermore, we found that the GLs growing in the North American Great Plains and the Eurasian continent west of Lake Balkhash to the Caspian Sea were significantly negatively correlated with temperature, and the cumulative response to temperature was relatively long (more than 4 months), which may be because the two regions belong to a temperate humid climate, and the increase in temperature significantly reduces soil moisture, which is unfavorable for local vegetation growth. In contrast, vegetation in arid regions has evolved mechanisms to withstand drought, allowing them to tolerate prolonged environmental anomalies [60]. The heterogeneous response durations of EBFs, OSs, CSs, Sava, WS, GLs, and CLs suggest complex temperature response mechanisms.

Increasing growing-season solar radiation enhances photosynthetic enzyme activity [58], providing more photosynthetically active radiation (PAR) to improve plant photosynthetic capacity and carbon sequestration [61,62]. Sunlight also delays leaf abscisic acid accumulation, slowing down aging and extending the growing season [63,64]. Wen et al. (2019) [28] documented that solar radiation promotes snow melting and indirectly increases surrounding temperatures, thus facilitating vegetation growth. However, this energy conversion process requires a certain accumulation period. It is likely why this study found that ENFs, DNFs, MFs, Sava, and WS, which are widely distributed in ARC and NTEM, had a strong or above-positive correlation with ATEM and ASOLAR, and they mainly exhibited a 0–1 month cumulative effect of temperature, while the cumulative effect of solar radiation mainly occurred within 2–3 months. This result further validates previous findings [28,48] that vegetation growth in ARC and NTEM can respond rapidly to temperature changes but requires a certain amount of accumulated solar radiation. This study found varying cumulative effects of solar radiation on vegetation growth in low-latitude arid and semi-arid regions, confirming previous research findings [15,48]. This relationship is closely related

to the complex vegetation composition in these regions. The growth of vegetation in these regions shows a negative correlation with ASOLAR. This could be because an increase in long-term solar radiation promotes evapotranspiration and leads to water loss, which is unfavorable for vegetation growth [24]. However, in the EBF of the Amazon rainforest, there is a high positive correlation with solar radiation, consistent with previous study [65], which indicates that solar radiation is an important driving factor for leaf shedding and new leaf growth in the Amazon rainforest. Additionally, this study's results suggest that the cumulative response of grasslands in the North American Great Plains to temperature and solar radiation is longer than that of grasslands in the Eurasian continent west of Lake Balkhash to the Caspian Sea. This indicates that grasslands in the Great Plains have developed stronger mechanisms to tolerate drought and light conditions. We believe this may be related to the widespread presence of C4 grasslands in North America, which have strong characteristics of adaptation to high temperatures, intense light, and arid environments [60].

This study found that, globally, the average OAT for vegetation types is generally ranked as precipitation > solar radiation > temperature, aligning with the research conducted by DING et al. [48]. Previous studies have indicated that green vegetation can adapt to seasonal variations in water, heat, and solar radiation resources through leaf shedding [66]. For tropical rain forests, the peak of leaf litter occurs during the dry spring or winter seasons and is predominantly regulated by precipitation and radiation, while for boreal forests, the peak of leaf litter occurs in different seasons and is mostly regulated by radiation and temperature [66]. Furthermore, studies have shown that temperature drives the distribution of deciduous and evergreen forests through its impact on nitrogen mineralization rates [67]. The effect of temperature on aboveground biomass accumulation in DBFs transitions from initial inhibition to subsequent promotion during the maturation stage [67]. Additionally, precipitation contributes to biomass accumulation in maturing ENFs but inhibits biomass accumulation in maturing EBFs, DNFs, and DBFs [67]. This indicates that different vegetation types exhibit complex and not absolute response mechanisms to climatic factors, which is also a major cause of spatiotemporal heterogeneity in cumulative climatic effects on global vegetation.

This study found stronger cumulative solar radiation effects, followed by temperature, and then precipitation, for widely distributed Arctic (ARC) vegetation types, including OSs, Sava, WS, and GLs, congruent with the results of SHI et al. [29]. DBFs, Sava, and WS exhibited prolonged intra-annual response durations, which is consistent with the findings of DING et al. [48]. This study indicates that the global distributions of the cumulative effects of climate on GLs and CLs, Sava and WS, and CSs and OSs share a similarity pattern, aligning with previous research [15,48]. This may be related to the similarity in community types, intrinsic characteristics, and growth environments shared by these vegetation types [10,68]. For Sava and WS, the cumulative effects of each climate factor in NTEM and STEM are more similar to those of OSs, but in TRP, they are more similar to those of GLs. This may be because in TRP, the NDVI information captured by satellites is mainly derived from grasslands, while in NTEM and STEM, it is more derived from trees [69]. CSs are predominantly distributed in STEM, while OSs are ubiquitous across climatic zones. This study reveals that there is no clear absolute advantage in the cumulative effects of precipitation on OSs and CSs, which is true also for solar radiation on CSs, indicating complex water and radiation demand for OSs' and CSs' growth [15,48]. Additionally, this study reveals that solar radiation mainly exhibits cumulative effects on OSs within 0–3 months, while temperature exhibits cumulative effects of 0 months on OSs and CSs, illustrating the urgent demand of different shrub categories for light and heat energy [15,48]. However, the specific reasons behind these effects need further investigation.

Combining the global distribution of four major crops as mapped by the Chinese Academy of Agricultural Sciences, it can be observed that (Figures A5–A7) different crops exhibit varying cumulative effects on temperature, precipitation, and solar radiation. For example, a larger proportion of corn, soybean, and wheat show cumulative effects of

precipitation lasting up to 12 months, while rice primarily shows 2–3 months. Rice exhibits cumulative effects of solar radiation mainly within 4–8 months, while corn and soybean show mainly within 4–6 months, and wheat exhibits shorter times (around 3–4 months). Additionally, four major crops exhibit cumulative effects on temperature mainly within 0 and around 6 months. It is worth noting that CLs are a vegetation type that is heavily influenced by human activities [70]. People cultivate different crops based on factors such as seasons, climate, soil conditions, and the water requirements of these crops, which can be met through irrigation [71]. The growth of CLs is also influenced by local weather conditions, pests and diseases, fertilizer application, and other factors [72–74]. These factors contribute to the complexity of the duration and relationships of climatic factors' cumulative effects on CLs, which may be more intricate than what is revealed in this study.

In summary, the intrinsic tolerance, resistance, and adaptation mechanisms evolved in diverse vegetation types over time, alongside shifts in water, thermal, and nutrient limitations imposed by changing climatic factors, represent critical determinants of the spatiotemporal heterogeneities in cumulative climatic effects across vegetation biomes. The present findings enrich the theoretical comprehension of vegetation–climate interactions, elucidating the intricate processes governing vegetative responses to climate change. These insights contribute to formulating strategies for addressing and increasing adaptation to climate change. However, it is important to note the complex, multifaceted nature of climate change impacts on vegetation. This study relied solely on linear modeling to characterize vegetation–climate linkages, potentially oversimplifying true interactions. Furthermore, quantitative assessments of anthropogenic effects, extreme events, and other disturbances were not conducted here. Future work could explore nonlinear techniques to further disentangle cumulative climatic effect traits across vegetation types. Examining additional climatic and non-climatic parameters (e.g., human activity, natural disturbances) is also needed to elucidate specific factors eliciting pronounced heterogeneous responses among tropical/Australian vegetation biomes, EBFs, OSs, CSs, Sava, WS, and CLs. This study spans over 30 years of data, and through comparative analyses of land use at the beginning and end of the study period, efforts were made to eliminate regions with significant changes in vegetation types during the research period. However, few pixels might still have exhibited land use changes that were not captured, which could have introduced a certain degree of error into the research results. Future research could attempt to further eliminate these pixels. In addition, global climate change is a complex phenomenon, with cumulative effects influenced by both natural and anthropogenic factors. This study only employed three main climatic factors to investigate the cumulative effects of climate change on vegetation growth, and, thus, our conclusions explain the main cumulative effects reflected by these climatic factors. Future research could incorporate more influencing factors, thereby more comprehensively characterizing this phenomenon. Furthermore, consistent with previous studies [28], heterogeneities exist in the desert of central Australia, as well as the African and the Amazon rainforests. The reason might be that NDVI is sensitive to soil background, which makes it difficult for the vegetation index based on red and near-infrared reflectance to distinguish perennial vegetation in arid and semi-arid ecosystems from the red soil, as these plants often lack contrast between red and near-infrared reflectance [75,76]. NDVI tends to saturate over regions like the Amazon rainforest, making it more susceptible to residual cloud or aerosol noise than other vegetation indices [77,78]. We argue and strongly recommend that field-based studies be conducted to reduce this confusion.

6. Conclusions

This study utilized accumulated temperature, precipitation, and solar radiation data, as well as GIMMS NDVI3g data, to examine the intra-annual cumulative climatic effects on global vegetation biomes from 1982 to 2015 quantitatively. The main conclusions are as follows.

Precipitation exerted the longest cumulative effects on vegetation growth worldwide with significant intra-annual heterogeneity. Specifically, precipitation primarily displayed

6–7 and 12-month cumulative effects on ENFs, 0–3- and 12-month effects on GLs and CLs, 2–3-month effects on DNFs, and up to 12-month effects on over 40% of DBFs and MFs. Solar radiation's cumulative effects on vegetation growth were concentrated within 0–6 months, with 3–5-month effects dominating in ENFs and DBFs and 3-month effects in DNFs and MFs. Temperature exhibited the shortest cumulative effects, with no significant impacts observed for many tree types. EBFs, CSs, OSs, Sava, and WS showed the most complex cumulative effects without a clear duration dominance. Vegetation types demonstrated weak-to-moderate correlations with APRE, highlighting the complex role of precipitation. Apart from EBFs, CSs, OSs, and Sava, other vegetation types showed strong-to-extremely-strong positive ATEM and ASOLAR correlations, indicating temperature and radiation dependency during growth cycles. This research indicates that the intrinsic tolerance, resistance, and adaptation mechanisms evolved in vegetation types over time, alongside shifting water, thermal, and nutrient limitations imposed by climate changes, are critical determinants of the spatiotemporal heterogeneities in intra-annual cumulative climatic effects. The results of this study provide key theoretical underpinnings to construct more accurate vegetation–climate relational models moving forward.

Author Contributions: G.D.: Data curation, Formal analysis, Software, Supervision, Writing—original draft, Writing—review and editing, Validation, Visualization. S.Y.: Data curation, Formal analysis, Software, Writing—original draft, Writing—review and editing, Validation, Visualization. H.C.: Resources, Supervision, Writing review and editing. J.Y.: Methodology, Resources, Supervision, Writing review and editing. Y.W.: Conceptualization, Methodology, Funding acquisition, Resources, Supervision, Writing original draft, Writing—review and editing. All authors have read and agreed to the published version of the manuscript.

Funding: This work was funded by the National Science Foundation for Young Scientists of China (No. 42007406), the Guangzhou Science and Technology Plan Project (No. 202102020666), the Guangdong Natural Science Foundation-General Program (No. 2022A1515010632), and the Fundamental Research Funds for the Central Public Welfare Research Institutes (No. PM-zx097-202305-214).

Data Availability Statement: Data are contained within the article.

Acknowledgments: The authors would like to thank the researchers who provided the opensource algorithms, which were extremely helpful to the research reported in this paper.

Conflicts of Interest: The authors declare no conflicts of interest.

Appendix A

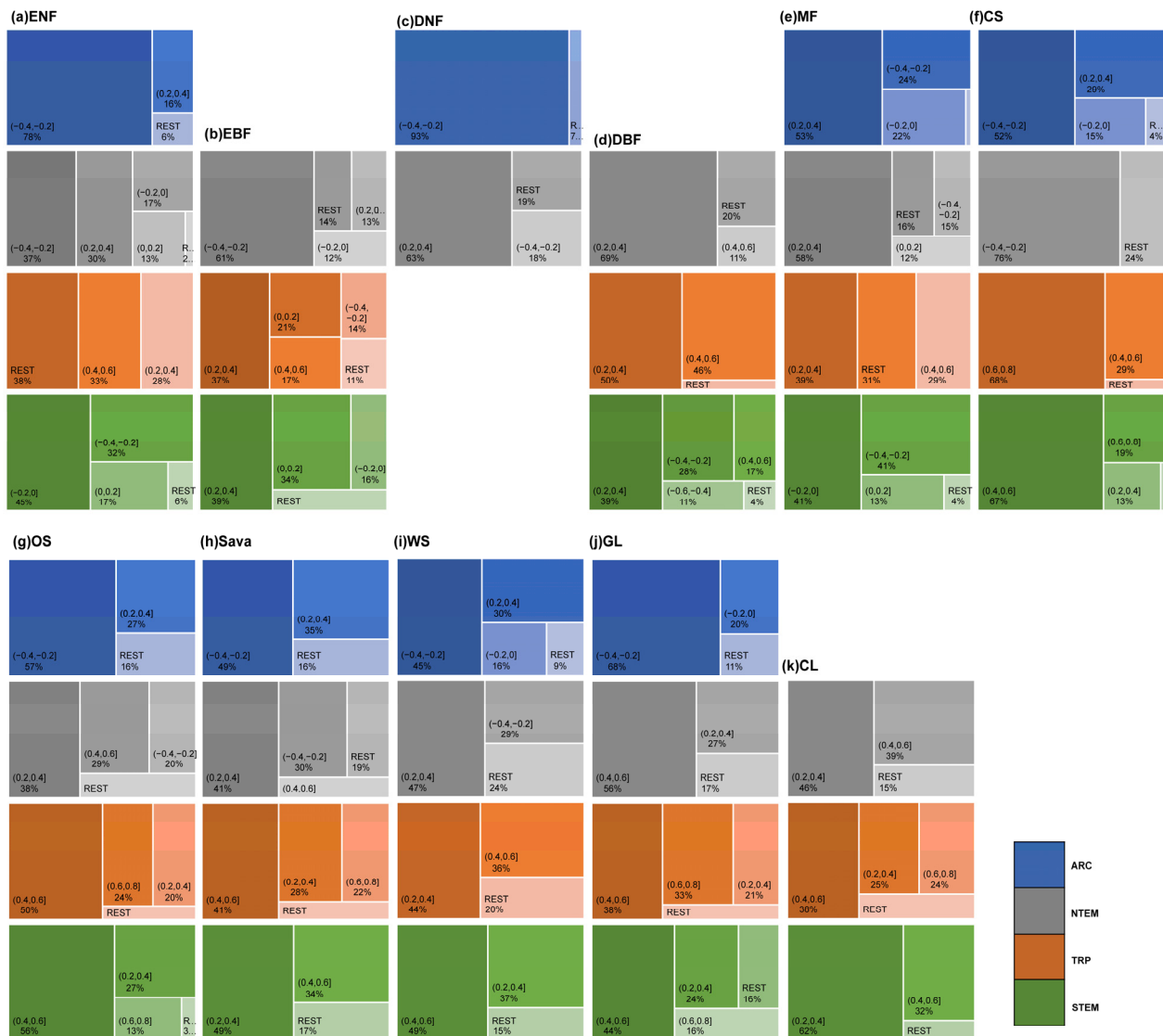


Figure A1. The rectangular tree map illustrates the proportion of the partial correlation strength between the growth of different vegetation types in various climatic zones and APRE. Different color schemes represent different climatic zones, and each vegetation type is labeled in the top left corner of the corresponding box. The map displays the large proportion of partial correlations and merges the smaller proportions into the category “REST”.

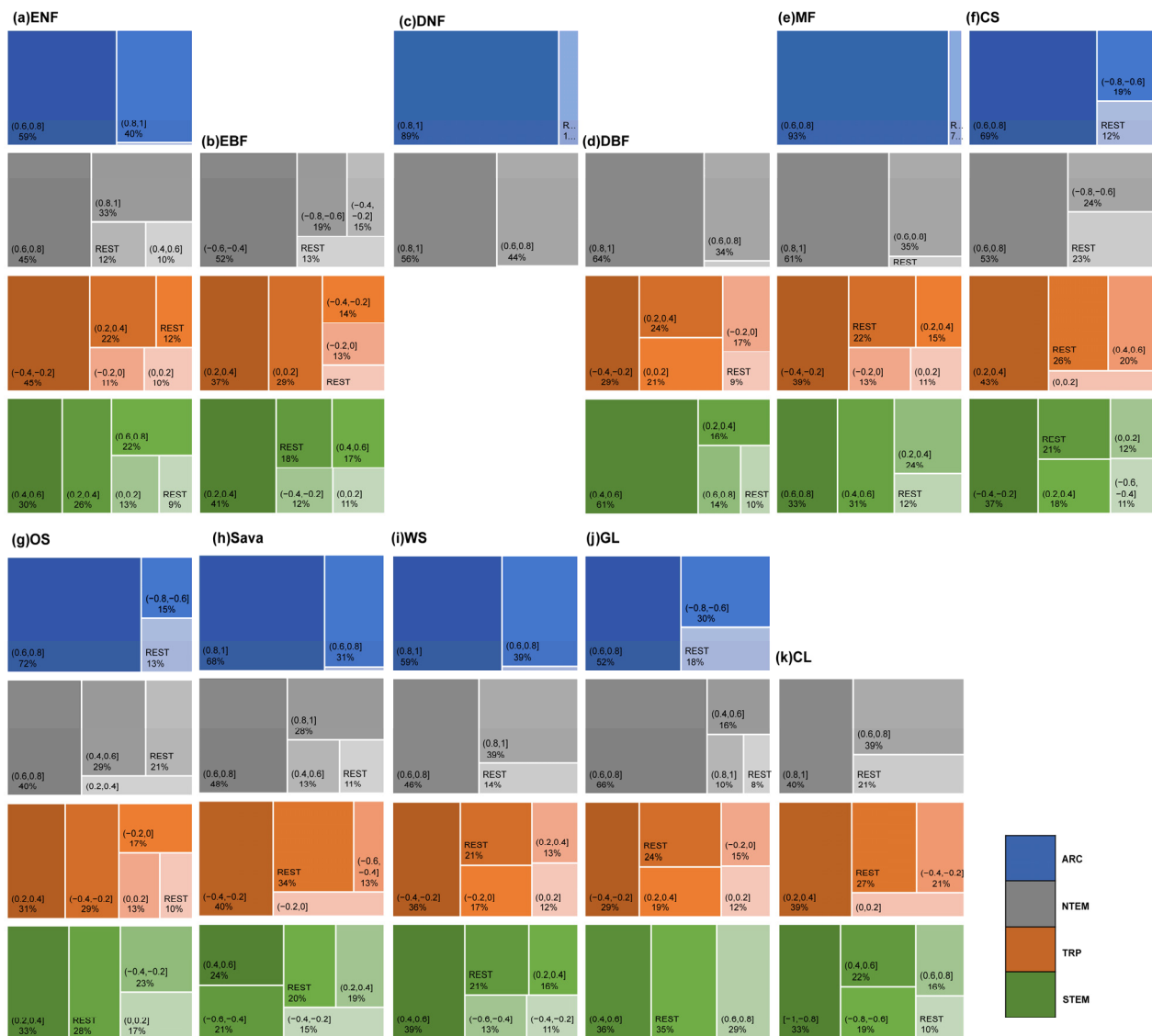


Figure A2. The rectangular tree map illustrates the proportion of the partial correlation strength between the growth of different vegetation types in various climatic zones and ASOLAR. Different color schemes represent different climatic zones, and each vegetation type is labeled in the top left corner of the corresponding box. The map displays the large proportion of partial correlations and merges the smaller proportions into the category "REST".

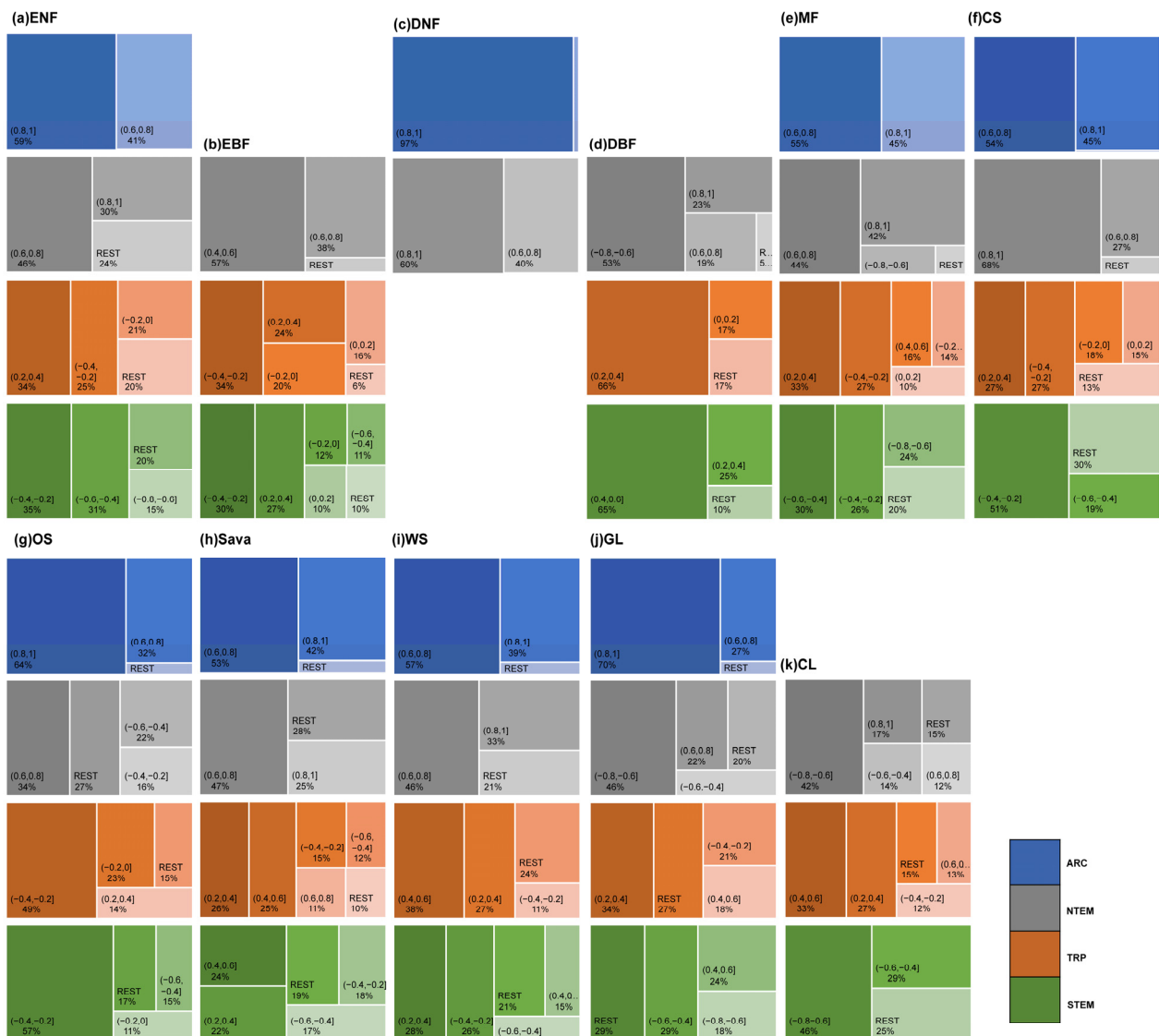


Figure A3. The rectangular tree map illustrates the proportion of the partial correlation strength between the growth of different vegetation types in various climatic zones and ATEM. Different color schemes represent different climatic zones, and each vegetation type is labeled in the top left corner of the corresponding box. The map displays the large proportion of partial correlations and merges the smaller proportions into the category “REST”.

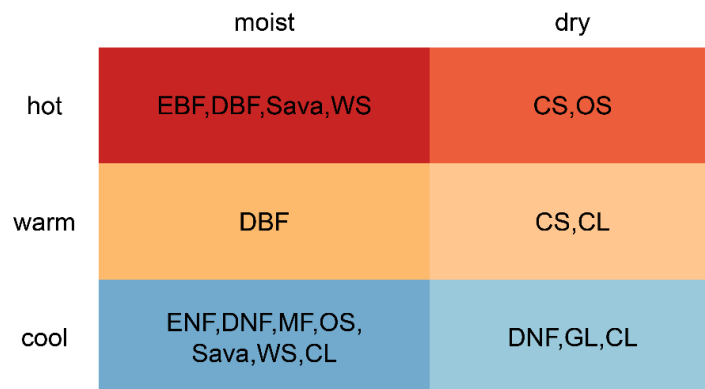


Figure A4. The climatic conditions of vegetation growth regions.

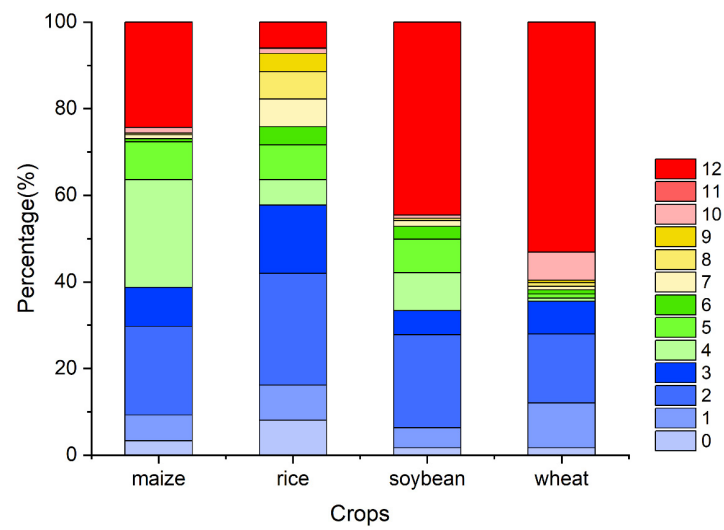


Figure A5. The percentage of the OAT of accumulation effects of precipitation on four major crops globally (maize, rice, soybean, and wheat).

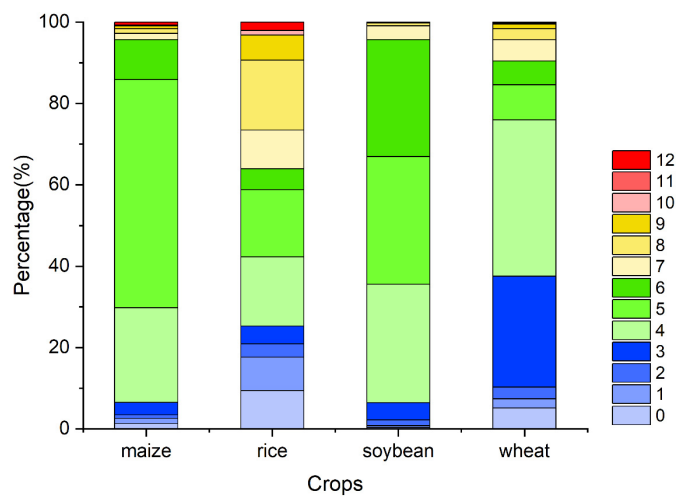


Figure A6. The percentage of the OAT of accumulation effects of solar radiation on four major crops globally (maize, rice, soybean, and wheat).

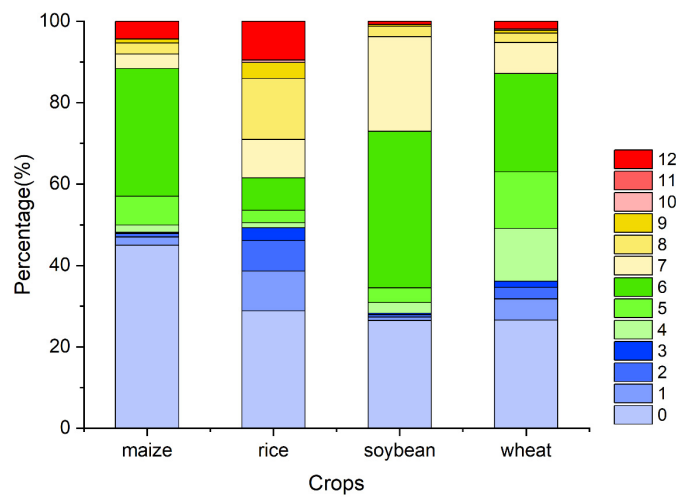


Figure A7. The percentage of the OAT of accumulation effects of temperature on four major crops globally (maize, rice, soybean, and wheat).

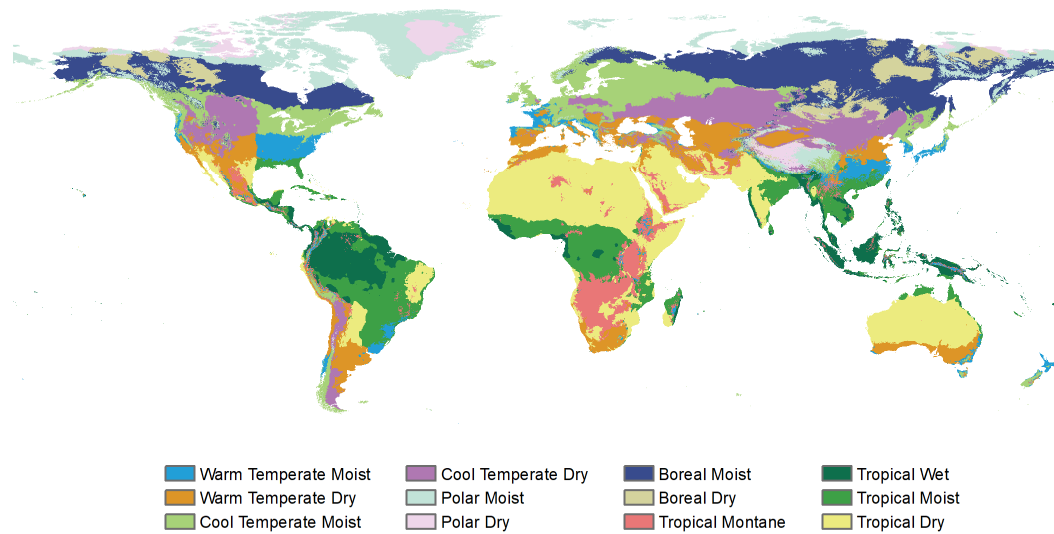


Figure A8. The climate zones defined by IPCC (<https://esdac.jrc.ec.europa.eu/projects/RenewableEnergy/>, accessed on 2 September 2023).

Table A1. Percentage of unchanged vegetation in different climate regions.

Climate Regions	ENF	EBF	DNF	DBF	MF	CS	OS	SAVA	WS	GL
Warm Temperate Moist	3.58%	2.51%	0.00%	38.55%	1.51%	0.02%	0.00%	4.36%	7.40%	0.64%
Warm Temperate Dry	0.42%	0.43%	0.00%	2.58%	0.27%	10.08%	13.33%	4.22%	2.86%	12.62%
Cool Temperate Moist	42.00%	0.41%	0.01%	42.37%	67.10%	0.99%	0.12%	5.74%	13.21%	6.92%
Cool Temperate Dry	1.89%	0.00%	0.00%	1.72%	2.13%	0.61%	3.12%	2.00%	1.86%	49.60%
Polar Moist	1.12%	0.00%	0.05%	0.02%	0.04%	7.69%	18.93%	1.16%	0.57%	5.80%
Polar Dry	0.00%	0.00%	0.00%	0.00%	0.00%	0.00%	1.90%	0.14%	0.01%	0.57%
Boreal Moist	48.18%	0.00%	63.71%	2.36%	24.73%	8.87%	17.91%	27.86%	40.07%	2.58%
Boreal Dry	2.61%	0.00%	36.23%	0.13%	4.08%	0.04%	2.19%	6.63%	9.46%	7.11%
Tropical Montane	0.03%	4.07%	0.00%	0.21%	0.01%	2.32%	4.32%	4.99%	7.83%	2.56%
Tropical Wet	0.00%	59.91%	0.00%	0.17%	0.00%	0.00%	0.00%	4.14%	2.66%	0.70%
Tropical Moist	0.16%	32.46%	0.00%	9.58%	0.12%	0.20%	0.01%	30.42%	10.13%	3.71%
Tropical Dry	0.00%	0.21%	0.00%	2.31%	0.00%	69.19%	38.17%	8.34%	3.95%	7.19%

Table A2. The proportion of the top ten optimal accumulation durations for APRE, ATEM, and ASOLAR across all climatic zones for different vegetation types.

Biomes	APRE			ATEM			ASOLAR		
	Time Accumulation	Climate Zones	Percentage	Time Accumulation	Climate Zones	Percentage	Time Accumulation	Climate Zones	Percentage
ENF	12	7	18.58%	0	7	46.48%	3	7	24.55%
	7	7	11.51%	0	3	27.52%	4	7	17.83%
	12	3	11.09%	7	3	5.00%	4	3	15.23%
	0	3	8.86%	6	3	4.31%	5	3	8.17%
	6	7	8.24%	0	8	2.43%	3	3	6.99%
	6	3	5.52%	1	3	1.19%	0	3	2.97%
	7	3	4.55%	5	3	1.12%	2	7	2.83%
	1	3	3.32%	0	4	1.06%	6	3	2.18%
	2	7	2.86%	0	0	0.96%	7	3	2.14%
	2	3	2.26%	0	5	0.89%	3	8	1.72%

Table A2. Cont.

Biomes	APRE			ATEM			ASOLAR		
	Time Accumulation	Climate Zones	Percentage	Time Accumulation	Climate Zones	Percentage	Time Accumulation	Climate Zones	Percentage
EBF	9	10	10.86%	0	10	19.09%	0	10	19.95%
	1	11	10.41%	0	11	14.67%	3	10	6.15%
	1	10	7.01%	1	10	8.01%	2	11	5.71%
	6	10	5.41%	1	11	6.90%	0	11	5.69%
	0	10	5.07%	5	10	5.58%	2	10	5.57%
	5	10	4.83%	6	10	4.37%	4	10	5.42%
	10	10	4.71%	7	10	4.06%	12	10	5.01%
	8	10	4.32%	2	10	3.62%	1	10	3.86%
	0	11	4.10%	12	10	3.33%	7	11	3.80%
	2	10	4.09%	4	10	2.88%	7	10	3.48%
DNF	2	7	35.10%	0	7	62.40%	3	7	61.57%
	2	8	12.12%	0	8	36.17%	3	8	35.50%
	7	8	11.87%	12	7	1.23%	4	7	1.13%
	12	7	10.54%	0	5	0.05%	2	7	0.69%
	7	7	9.36%	12	8	0.05%	4	8	0.49%
	3	8	6.84%	5	7	0.03%	0	7	0.22%
	3	7	3.97%	4	7	0.03%	2	8	0.21%
	8	7	2.08%	0	0	0.02%	9	7	0.10%
	12	8	1.92%	1	7	0.02%	3	5	0.05%
	8	8	1.54%	0	3	0.01%	3	0	0.01%
DBF	12	1	22.93%	0	3	29.25%	5	1	21.41%
	12	3	15.98%	6	1	26.05%	4	3	17.19%
	2	3	7.49%	7	1	8.93%	3	3	15.17%
	1	11	6.52%	6	3	5.53%	4	1	13.67%
	6	1	6.37%	7	3	5.36%	5	3	7.20%
	0	3	5.01%	8	11	2.62%	1	11	2.64%
	7	3	4.68%	0	7	2.18%	6	1	2.39%
	5	1	3.32%	3	11	2.17%	2	11	2.13%
	3	3	3.18%	0	1	1.66%	3	7	1.29%
	12	2	1.72%	0	0	1.31%	5	2	1.24%
MF	12	3	41.80%	0	3	55.77%	3	3	44.82%
	12	7	11.61%	0	7	24.14%	3	7	18.89%
	7	3	6.04%	6	3	6.56%	4	3	16.63%
	6	3	5.40%	0	8	4.00%	4	7	4.09%
	0	3	5.09%	7	3	2.99%	3	8	2.85%
	2	7	4.37%	0	4	1.83%	5	3	2.61%
	7	7	2.81%	0	0	0.50%	3	4	1.51%
	2	3	2.79%	6	1	0.46%	2	7	1.25%
	12	8	2.46%	5	3	0.43%	4	8	0.84%
	10	3	1.77%	7	1	0.33%	6	3	0.62%
CS	9	12	19.17%	0	12	25.29%	6	12	13.12%
	10	12	9.83%	12	12	16.26%	5	12	9.33%
	5	12	9.19%	0	7	7.22%	10	12	9.01%
	7	12	7.39%	0	5	6.53%	7	12	8.75%
	8	12	5.88%	4	12	5.36%	12	12	8.57%
	7	7	5.78%	8	12	4.64%	4	12	7.81%
	6	12	5.37%	7	12	4.27%	0	7	4.43%
	4	12	5.04%	3	12	3.68%	0	12	3.78%
	7	5	2.84%	0	2	2.62%	4	5	3.29%
	3	12	2.55%	7	2	2.31%	7	2	3.07%

Table A2. Cont.

Biomes	APRE			ATEM			ASOLAR		
	Time Accumulation	Climate Zones	Percentage	Time Accumulation	Climate Zones	Percentage	Time Accumulation	Climate Zones	Percentage
OS	9	12	8.11%	0	7	14.68%	3	7	12.24%
	8	5	5.13%	0	5	10.35%	3	5	9.07%
	12	7	4.84%	0	12	8.55%	12	12	7.53%
	8	12	4.82%	1	5	8.27%	2	5	7.04%
	5	12	4.80%	12	12	7.86%	7	12	6.02%
	3	12	4.37%	0	2	5.00%	6	12	5.06%
	7	12	4.23%	7	12	3.49%	0	12	4.66%
	8	7	3.59%	3	12	3.47%	10	12	4.51%
	4	12	3.57%	1	7	3.06%	2	7	3.01%
	10	12	2.72%	7	2	2.31%	8	12	2.78%
Sava	7	7	10.09%	0	7	27.11%	3	7	19.42%
	12	7	6.67%	0	3	2.88%	2	11	5.72%
	1	11	5.56%	0	8	6.38%	4	7	5.23%
	2	11	4.80%	6	1	1.47%	3	8	4.87%
	5	11	4.17%	3	9	0.75%	1	11	4.46%
	12	8	3.36%	0	11	7.79%	6	11	3.31%
	2	7	3.28%	7	1	0.41%	7	11	2.92%
	4	11	2.97%	2	11	2.75%	3	11	2.57%
	6	11	2.69%	12	1	0.75%	0	11	2.32%
	0	11	2.67%	4	9	0.58%	9	11	2.20%
WS	7	7	11.53%	0	7	38.95%	3	7	28.37%
	12	7	9.28%	0	3	9.85%	4	7	8.88%
	2	7	8.01%	0	8	9.07%	3	8	7.36%
	12	3	4.99%	6	1	2.12%	3	3	5.31%
	6	7	4.81%	3	9	1.93%	4	3	4.92%
	12	8	4.14%	0	11	1.70%	1	9	2.25%
	0	9	3.10%	7	1	1.63%	6	1	1.88%
	12	1	2.53%	2	11	1.46%	5	1	1.80%
	1	11	2.21%	12	1	1.40%	4	1	1.62%
	2	8	1.85%	4	9	1.39%	2	7	1.55%
GL	12	4	27.98%	3	4	10.99%	4	4	13.73%
	2	4	12.70%	4	4	10.97%	3	4	11.99%
	1	4	5.54%	0	4	7.34%	2	4	11.38%
	12	8	3.40%	6	4	5.73%	5	4	6.47%
	2	8	3.30%	5	4	5.23%	4	8	4.37%
	2	5	3.17%	0	8	4.91%	3	5	2.93%
	12	2	3.14%	0	5	3.70%	6	2	2.85%
	2	2	2.76%	6	2	3.53%	5	2	2.31%
	2	12	2.40%	2	4	2.82%	6	4	2.07%
	1	12	1.87%	0	3	2.51%	4	3	2.06%
CL	12	4	16.54%	0	4	12.77%	4	4	15.87%
	12	3	11.54%	6	3	8.76%	3	3	7.85%
	12	2	8.19%	0	3	7.58%	3	4	7.23%
	2	2	5.99%	6	4	5.47%	4	3	6.51%
	1	4	5.09%	0	2	5.46%	4	2	6.42%
	2	4	4.87%	4	4	5.10%	5	2	5.67%
	3	2	3.38%	5	4	4.59%	5	4	4.95%
	12	1	3.07%	6	2	4.54%	5	3	4.82%
	2	12	2.69%	6	1	4.44%	6	2	4.09%
	1	2	2.67%	5	2	3.57%	5	1	2.93%

Note: Climate regions: 1: Tropical Montane; 2: Tropical Wet; 3: Tropical Moist; 4: Tropical Dry; 5: Warm Temperate Moist; 6: Warm Temperate Dry; 7: Cool Temperate Moist; 8: Cool Temperate Dry; 9: Boreal Moist; 10: Boreal Dry; 11: Polar Moist; 12: Polar Dry.

References

- Buitenwerf, R.; Rose, L.; Higgins, S.I. Three decades of multi-dimensional change in global leaf phenology. *Nat. Clim. Chang.* **2015**, *5*, 364–368. [[CrossRef](#)]
- Peñuelas, J.; Filella, I. Responses to a Warming World. *Science* **2001**, *294*, 793–795. [[CrossRef](#)] [[PubMed](#)]
- Zhang, G.; Zhang, Y.; Dong, J.; Xiao, X. Green-up dates in the Tibetan Plateau have continuously advanced from 1982 to 2011. *Proc. Natl. Acad. Sci. USA* **2013**, *110*, 4309–4314. [[CrossRef](#)] [[PubMed](#)]
- Nemani, R.R.; Keeling, C.D.; Hashimoto, H.; Jolly, W.M.; Piper, S.C.; Tucker, C.J.; Myneni, R.B.; Running, S.W. Climate-Driven Increases in Global Terrestrial Net Primary Production from 1982 to 1999. *Science* **2003**, *300*, 1560–1563. [[CrossRef](#)]
- Ostberg, S.; Lucht, W.; Schaphoff, S.; Gerten, D. Critical impacts of global warming on land ecosystems. *Earth Syst. Dynam.* **2013**, *4*, 347–357. [[CrossRef](#)]
- Ciais, P.; Reichstein, M.; Viovy, N.; Granier, A.; Ogée, J.; Allard, V.; Aubinet, M.; Buchmann, N.; Bernhofer, C.; Carrara, A.; et al. Europe-wide reduction in primary productivity caused by the heat and drought in 2003. *Nature* **2005**, *437*, 529–533. [[CrossRef](#)]
- Gatti, L.V.; Gloor, M.; Miller, J.B.; Doughty, C.E.; Malhi, Y.; Domingues, L.G.; Basso, L.S.; Martinewski, A.; Correia, C.S.C.; Borges, V.F.; et al. Drought sensitivity of Amazonian carbon balance revealed by atmospheric measurements. *Nature* **2014**, *506*, 76–80. [[CrossRef](#)]
- Zhao, M.; Running, S.W. Drought-Induced Reduction in Global Terrestrial Net Primary Production from 2000 Through 2009. *Science* **2010**, *329*, 940–943. [[CrossRef](#)]
- de Jong, R.; Schaepman, M.E.; Furrer, R.; de Bruin, S.; Verburg, P.H. Spatial relationship between climatologies and changes in global vegetation activity. *Glob. Chang. Biol.* **2013**, *19*, 1953–1964. [[CrossRef](#)]
- Woodward, F.I.; Lomas, M.R.; Kelly, C.K. Global climate and the distribution of plant biomes. *Philos. Trans. R. Soc. London Ser. B Biol. Sci.* **2004**, *359*, 1465–1476. [[CrossRef](#)]
- Fu, G.; Sun, W.; Li, S.; Zhang, J.; Yu, C.; Shen, Z. Modeling Aboveground Biomass Using MODIS Images and Climatic Data in Grasslands on the Tibetan Plateau. *J. Resour. Ecol.* **2017**, *8*, 42–49. [[CrossRef](#)]
- Garbulsky, M.F.; Peñuelas, J.; Papale, D.; Ardo, J.; Goulden, M.L.; Kiely, G.; Richardson, A.D.; Rotenberg, E.; Veenendaal, E.M.; Filella, I. Patterns and controls of the variability of radiation use efficiency and primary productivity across terrestrial ecosystems. *Glob. Ecol. Biogeogr.* **2010**, *19*, 253–267. [[CrossRef](#)]
- Musau, J.; Patil, S.; Sheffield, J.; Marshall, M. Spatio-temporal vegetation dynamics and relationship with climate over East Africa. *Hydrol. Earth Syst. Sci. Discuss.* **2016**, *2016*, 1–30. [[CrossRef](#)]
- Zhu, L.; Southworth, J. Disentangling the Relationships between Net Primary Production and Precipitation in Southern Africa Savannas Using Satellite Observations from 1982 to 2010. *Remote Sens.* **2013**, *5*, 3803–3825. [[CrossRef](#)]
- Wu, D.; Zhao, X.; Liang, S.; Zhou, T.; Huang, K.; Tang, B.; Zhao, W. Time-lag effects of global vegetation responses to climate change. *Glob. Chang. Biol.* **2015**, *21*, 3520–3531. [[CrossRef](#)]
- Xu, G.; Zhang, H.; Chen, B.; Zhang, H.; Innes, J.L.; Wang, G.; Yan, J.; Zheng, Y.; Zhu, Z.; Myneni, R.B. Changes in Vegetation Growth Dynamics and Relations with Climate over China's Landmass from 1982 to 2011. *Remote Sens.* **2014**, *6*, 3263–3283. [[CrossRef](#)]
- Zhao, W.; Zhao, X.; Zhou, T.; Wu, D.; Tang, B.; Wei, H. Climatic factors driving vegetation declines in the 2005 and 2010 Amazon droughts. *PLoS ONE* **2017**, *12*, e0175379. [[CrossRef](#)]
- Papagiannopoulou, C.; Miralles, D.G.; Dorigo, W.A.; Verhoest, N.E.C.; Depoorter, M.; Waegeman, W. Vegetation anomalies caused by antecedent precipitation in most of the world. *Environ. Res. Lett.* **2017**, *12*, 074016. [[CrossRef](#)]
- Sherry, R.A.; Weng, E.; Arnone III, J.A.; Johnson, D.W.; Schimel, D.S.; Verburg, P.S.; Wallace, L.L.; Luo, Y. Lagged effects of experimental warming and doubled precipitation on annual and seasonal aboveground biomass production in a tallgrass prairie. *Glob. Chang. Biol.* **2008**, *14*, 2923–2936. [[CrossRef](#)]
- Kuzyakov, Y.; Gavrichkova, O. REVIEW: Time lag between photosynthesis and carbon dioxide efflux from soil: A review of mechanisms and controls. *Glob. Chang. Biol.* **2010**, *16*, 3386–3406. [[CrossRef](#)]
- Braswell, B.H.; Schimel, D.S.; Linder, E.; Moore, B. The Response of Global Terrestrial Ecosystems to Interannual Temperature Variability. *Science* **1997**, *278*, 870–873. [[CrossRef](#)]
- Vukićević, T.; Braswell, B.H.; Schimel, D. A diagnostic study of temperature controls on global terrestrial carbon exchange. *Tellus B* **2001**, *53*, 150–170. [[CrossRef](#)]
- Zhang, T.; Yang, S.; Guo, R.; Guo, J. Correction: Warming and Nitrogen Addition Alter Photosynthetic Pigments, Sugars and Nutrients in a Temperate Meadow Ecosystem. *PLoS ONE* **2016**, *11*, e0158249. [[CrossRef](#)]
- Vicente-Serrano, S.M.; Gouveia, C.; Camarero, J.J.; Beguería, S.; Trigo, R.; López-Moreno, J.I.; Azorín-Molina, C.; Pasho, E.; Lorenzo-Lacruz, J.; Revuelto, J.; et al. Response of vegetation to drought time-scales across global land biomes. *Proc. Natl. Acad. Sci. USA* **2013**, *110*, 52–57. [[CrossRef](#)]
- Gunderson, C.A.; Norby, R.J.; Wullschlegel, S.D. Acclimation of photosynthesis and respiration to simulated climatic warming in northern and southern populations of *Acer saccharum*: Laboratory and field evidence. *Tree Physiol.* **2000**, *20*, 87–96. [[CrossRef](#)]
- Slot, M.; Kitajima, K. General patterns of acclimation of leaf respiration to elevated temperatures across biomes and plant types. *Oecologia* **2015**, *177*, 885–900. [[CrossRef](#)]
- Yamori, W.; Hikosaka, K.; Way, D.A. Temperature response of photosynthesis in C3, C4, and CAM plants: Temperature acclimation and temperature adaptation. *Photosynth. Res.* **2014**, *119*, 101–117. [[CrossRef](#)] [[PubMed](#)]

28. Wen, Y.; Liu, X.; Xin, Q.; Wu, J.; Xu, X.; Pei, F.; Li, X.; Du, G.; Cai, Y.; Lin, K.; et al. Cumulative Effects of Climatic Factors on Terrestrial Vegetation Growth. *J. Geophys. Res. Biogeosci.* **2019**, *124*, 789–806. [[CrossRef](#)]
29. Shi, S.; Wang, P.; Zhang, Y.; Yu, J. Cumulative and time-lag effects of the main climate factors on natural vegetation across Siberia. *Ecol. Indic.* **2021**, *133*, 108446. [[CrossRef](#)]
30. Sun, Q.; Liu, C.; Chen, T.; Zhang, A. A Weighted-Time-Lag Method to Detect Lag Vegetation Response to Climate Variation: A Case Study in Loess Plateau, China, 1982–2013. *Remote Sens.* **2021**, *13*, 923. [[CrossRef](#)]
31. Wei, X.; He, W.; Zhou, Y.; Ju, W.; Xiao, J.; Li, X.; Liu, Y.; Xu, S.; Bi, W.; Zhang, X.; et al. Global assessment of lagged and cumulative effects of drought on grassland gross primary production. *Ecol. Indic.* **2022**, *136*, 108646. [[CrossRef](#)]
32. Wu, C.; Wang, T. Evaluating Cumulative Drought Effect on Global Vegetation Photosynthesis Using Numerous GPP Products. *Front. Environ. Sci.* **2022**, *10*, 908875. [[CrossRef](#)]
33. Yuan, Y.; Bao, A.; Jiapaer, G.; Jiang, L.; De Maeyer, P. Phenology-based seasonal terrestrial vegetation growth response to climate variability with consideration of cumulative effect and biological carryover. *Sci. Total Environ.* **2022**, *817*, 152805. [[CrossRef](#)]
34. Zhao, A.; Yu, Q.; Feng, L.; Zhang, A.; Pei, T. Evaluating the cumulative and time-lag effects of drought on grassland vegetation: A case study in the Chinese Loess Plateau. *J. Environ. Manag.* **2020**, *261*, 110214. [[CrossRef](#)]
35. Liu, H.; Zhang, A.; Liu, C.; Zhao, Y.; Zhao, A.; Wang, D. Analysis of the time-lag effects of climate factors on grassland productivity in Inner Mongolia. *Glob. Ecol. Conserv.* **2021**, *30*, e01751. [[CrossRef](#)]
36. Peng, S.; Piao, S.; Ciais, P.; Myneni, R.B.; Chen, A.; Chevallier, F.; Dolman, A.J.; Janssens, I.A.; Peñuelas, J.; Zhang, G.; et al. Asymmetric effects of daytime and night-time warming on Northern Hemisphere vegetation. *Nature* **2013**, *501*, 88–92. [[CrossRef](#)]
37. Piao, S.; Tan, J.; Chen, A.; Fu, Y.H.; Ciais, P.; Liu, Q.; Janssens, I.A.; Vicca, S.; Zeng, Z.; Jeong, S.-J.; et al. Leaf onset in the northern hemisphere triggered by daytime temperature. *Nat. Commun.* **2015**, *6*, 6911. [[CrossRef](#)]
38. Tan, J.; Piao, S.; Chen, A.; Zeng, Z.; Ciais, P.; Janssens, I.A.; Mao, J.; Myneni, R.B.; Peng, S.; Peñuelas, J.; et al. Seasonally different response of photosynthetic activity to daytime and night-time warming in the Northern Hemisphere. *Glob. Chang. Biol.* **2015**, *21*, 377–387. [[CrossRef](#)]
39. Piao, S.; Friedlingstein, P.; Ciais, P.; Viovy, N.; Demarty, J. Growing season extension and its impact on terrestrial carbon cycle in the Northern Hemisphere over the past 2 decades. *Glob. Biogeochem. Cycles* **2007**, *21*, GB3018. [[CrossRef](#)]
40. Harris, I.; Jones, P.D.; Osborn, T.J.; Lister, D.H. Updated high-resolution grids of monthly climatic observations—The CRU TS3.10 Dataset. *Int. J. Climatol.* **2014**, *34*, 623–642. [[CrossRef](#)]
41. Stackhouse Jr, P.; Gupta, S.; Cox, S.; Mikovitz, J.C.; Zhang, T.; Chiacchio, M. 12-year surface radiation budget data set. *GEWEX News* **2004**, *14*, 10–12.
42. Müller Schmied, H.; Müller, R.; Sanchez-Lorenzo, A.; Ahrens, B.; Wild, M. Evaluation of Radiation Components in a Global Freshwater Model with Station-Based Observations. *Water* **2016**, *8*, 450. [[CrossRef](#)]
43. Sheffield, J.; Wood, E.F.; Roderick, M.L. Little change in global drought over the past 60 years. *Nature* **2012**, *491*, 435–438. [[CrossRef](#)]
44. Wu, X.; Liu, H.; Li, X.; Liang, E.; Beck, P.S.A.; Huang, Y. Seasonal divergence in the interannual responses of Northern Hemisphere vegetation activity to variations in diurnal climate. *Sci. Rep.* **2016**, *6*, 19000. [[CrossRef](#)] [[PubMed](#)]
45. De Fries, R.S.; Hansen, M.; Townshend, J.R.G.; Sohlberg, R. Global land cover classifications at 8 km spatial resolution: The use of training data derived from Landsat imagery in decision tree classifiers. *Int. J. Remote Sens.* **1998**, *19*, 3141–3168. [[CrossRef](#)]
46. Barnes, M.L.; Moran, M.S.; Scott, R.L.; Kolb, T.E.; Ponce-Campos, G.E.; Moore, D.J.P.; Ross, M.A.; Mitra, B.; Dore, S. Vegetation productivity responds to sub-annual climate conditions across semiarid biomes. *Ecosphere* **2016**, *7*, e01339. [[CrossRef](#)]
47. Wen, Y.; Liu, X.; Du, G. Nonuniform Time-Lag Effects of Asymmetric Warming on Net Primary Productivity across Global Terrestrial Biomes. *Earth Interact.* **2018**, *22*, 1–26. [[CrossRef](#)]
48. Ding, Y.; Li, Z.; Peng, S. Global analysis of time-lag and -accumulation effects of climate on vegetation growth. *Int. J. Appl. Earth Obs. Geoinf.* **2020**, *92*, 102179. [[CrossRef](#)]
49. Aubin, I.; Munson, A.D.; Cardou, F.; Burton, P.J.; Isabel, N.; Pedlar, J.H.; Paquette, A.; Taylor, A.R.; Delagrangé, S.; Kebli, H.; et al. Traits to stay, traits to move: A review of functional traits to assess sensitivity and adaptive capacity of temperate and boreal trees to climate change. *Environ. Rev.* **2016**, *24*, 164–186. [[CrossRef](#)]
50. Anderegg, L.D.L.; HilleRisLambers, J. Drought stress limits the geographic ranges of two tree species via different physiological mechanisms. *Glob. Chang. Biol.* **2016**, *22*, 1029–1045. [[CrossRef](#)]
51. Mayoral, C.; Pardos, M.; Sánchez-González, M.; Brendel, O.; Pita, P. Ecological implications of different water use strategies in three coexisting mediterranean tree species. *For. Ecol. Manag.* **2016**, *382*, 76–87. [[CrossRef](#)]
52. Pardos, M.; del Río, M.; Pretzsch, H.; Jactel, H.; Bielak, K.; Bravo, F.; Brazaitis, G.; Defosse, E.; Engel, M.; Godvold, K.; et al. The greater resilience of mixed forests to drought mainly depends on their composition: Analysis along a climate gradient across Europe. *For. Ecol. Manag.* **2021**, *481*, 118687. [[CrossRef](#)]
53. Liu, Y.; Liu, R.; Pisek, J.; Chen, J.M. Separating overstory and understory leaf area indices for global needleleaf and deciduous broadleaf forests by fusion of MODIS and MISR data. *Biogeosciences* **2017**, *14*, 1093–1110. [[CrossRef](#)]
54. Ershadi, A.; McCabe, M.F.; Evans, J.P.; Wood, E.F. Impact of model structure and parameterization on Penman–Monteith type evaporation models. *J. Hydrol.* **2015**, *525*, 521–535. [[CrossRef](#)]

55. Gang, C.; Zhou, W.; Wang, Z.; Chen, Y.; Li, J.; Chen, J.; Qi, J.; Odeh, I.; Groisman, P.Y. Comparative Assessment of Grassland NPP Dynamics in Response to Climate Change in China, North America, Europe and Australia from 1981 to 2010. *J. Agron. Crop Sci.* **2015**, *201*, 57–68. [[CrossRef](#)]
56. Aouissi, J.; Benabdallah, S.; Lili Chabaâne, Z.; Cudennec, C. Evaluation of potential evapotranspiration assessment methods for hydrological modelling with SWAT—Application in data-scarce rural Tunisia. *Agric. Water Manag.* **2016**, *174*, 39–51. [[CrossRef](#)]
57. Liu, N.; Shi, Y.; Ding, Y.; Liu, L.; Peng, S. Temporal effects of climatic factors on vegetation phenology on the Loess Plateau, China. *J. Plant Ecol.* **2023**, *16*, rtac063. [[CrossRef](#)]
58. Shi, C.; Sun, G.; Zhang, H.; Xiao, B.; Ze, B.; Zhang, N.; Wu, N. Effects of Warming on Chlorophyll Degradation and Carbohydrate Accumulation of Alpine Herbaceous Species during Plant Senescence on the Tibetan Plateau. *PLoS ONE* **2014**, *9*, e107874. [[CrossRef](#)]
59. Fracheboud, Y.; Luquez, V.; Björkén, L.; Sjödin, A.; Tuominen, H.; Jansson, S. The Control of Autumn Senescence in European Aspen. *Plant Physiol.* **2009**, *149*, 1982–1991. [[CrossRef](#)]
60. Ke, Y.; Leung, L.R.; Huang, M.; Coleman, A.M.; Li, H.; Wigmosta, M.S. Development of high resolution land surface parameters for the Community Land Model. *Geosci. Model Dev.* **2012**, *5*, 1341–1362. [[CrossRef](#)]
61. Kim, J.-H.; Moon, Y.R.; Wi, S.G.; Kim, J.-S.; Lee, M.H.; Chung, B.Y. Differential Radiation Sensitivities of Arabidopsis Plants at Various Developmental Stages. In *Photosynthesis. Energy from the Sun: Proceedings of the 14th International Congress on Photosynthesis, Glasgow, UK, 22–27 July 2007*; Springer: Dordrecht, The Netherlands, 2008; pp. 1491–1495.
62. He, P.; Osaki, M.; Takebe, M.; Shinano, T.; Wasaki, J. Endogenous hormones and expression of senescence-related genes in different senescent types of maize. *J. Exp. Bot.* **2005**, *56*, 1117–1128. [[CrossRef](#)] [[PubMed](#)]
63. Liu, Q.; Fu, Y.H.; Zeng, Z.; Huang, M.; Li, X.; Piao, S. Temperature, precipitation, and insolation effects on autumn vegetation phenology in temperate China. *Glob. Chang. Biol.* **2016**, *22*, 644–655. [[CrossRef](#)] [[PubMed](#)]
64. Gepstein, S.; Thimann, K.V. Changes in the abscisic acid content of oat leaves during senescence. *Proc. Natl. Acad. Sci. USA* **1980**, *77*, 2050–2053. [[CrossRef](#)] [[PubMed](#)]
65. Chen, X.; Ciais, P.; Maignan, F.; Zhang, Y.; Bastos, A.; Liu, L.; Bacour, C.; Fan, L.; Gentine, P.; Goll, D.; et al. Vapor Pressure Deficit and Sunlight Explain Seasonality of Leaf Phenology and Photosynthesis Across Amazonian Evergreen Broadleaved Forest. *Glob. Biogeochem. Cycles* **2021**, *35*, e2020GB006893. [[CrossRef](#)]
66. Zhang, H.; Yuan, W.; Dong, W.; Liu, S. Seasonal patterns of litterfall in forest ecosystem worldwide. *Ecol. Complex.* **2014**, *20*, 240–247. [[CrossRef](#)]
67. Weng, E.; Farrior, C.E.; Dybzinski, R.; Pacala, S.W. Predicting vegetation type through physiological and environmental interactions with leaf traits: Evergreen and deciduous forests in an earth system modeling framework. *Glob. Chang. Biol.* **2017**, *23*, 2482–2498. [[CrossRef](#)]
68. Loidi, J.; Navarro-Sánchez, G.; Vynokurov, D. Climatic definitions of the world’s terrestrial biomes. *Veg. Classif. Surv.* **2022**, *3*, 231–271. [[CrossRef](#)]
69. Lehmann, C.E.R.; Archibald, S.A.; Hoffmann, W.A.; Bond, W.J. Deciphering the distribution of the savanna biome. *New Phytol.* **2011**, *191*, 197–209. [[CrossRef](#)]
70. Shi, X.; Wang, W.; Shi, W. Progress on quantitative assessment of the impacts of climate change and human activities on cropland change. *J. Geogr. Sci.* **2016**, *26*, 339–354. [[CrossRef](#)]
71. Frisvold, G.B.; Konyar, K. Climate Change Mitigation Policies: Implications for Agriculture and Water Resources. *J. Contemp. Water Res. Educ.* **2013**, *151*, 27–42. [[CrossRef](#)]
72. Chen, Q.; Yang, L.E.; Luo, J.; Liu, F.; Zhang, Y.; Zhou, Q.; Guo, R.; Gu, X. The 300 years cropland changes reflecting climate impacts and social resilience at the Yellow River–Huangshui River Valley, China. *Environ. Res. Lett.* **2021**, *16*, 065006. [[CrossRef](#)]
73. Mueller, N.D.; Butler, E.E.; McKinnon, K.A.; Rhines, A.; Tingley, M.; Holbrook, N.M.; Huybers, P. Cooling of US Midwest summer temperature extremes from cropland intensification. *Nat. Clim. Chang.* **2016**, *6*, 317–322. [[CrossRef](#)]
74. Reinermann, S.; Gessner, U.; Asam, S.; Kuenzer, C.; Dech, S. The Effect of Droughts on Vegetation Condition in Germany: An Analysis Based on Two Decades of Satellite Earth Observation Time Series and Crop Yield Statistics. *Remote Sens.* **2019**, *11*, 1783. [[CrossRef](#)]
75. Jafari, R.; Lewis, M.M.; Ostendorf, B. Evaluation of vegetation indices for assessing vegetation cover in southern arid lands in South Australia. *Rangel. J.* **2007**, *29*, 39–49. [[CrossRef](#)]
76. Leprieux, C.; Kerr, Y.H.; Mastorchio, S.; Meunier, J.C. Monitoring vegetation cover across semi-arid regions: Comparison of remote observations from various scales. *Int. J. Remote Sens.* **2000**, *21*, 281–300. [[CrossRef](#)]
77. Brantley, S.T.; Zinnert, J.C.; Young, D.R. Application of hyperspectral vegetation indices to detect variations in high leaf area index temperate shrub thicket canopies. *Remote Sens. Environ.* **2011**, *115*, 514–523. [[CrossRef](#)]
78. Zhang, Y.; Tian, Y.; Knyazikhin, Y.; Martonchik, J.V.; Diner, D.J.; Leroy, M.; Myneni, R.B.; Sensing, R. Prototyping of MISR LAI and FPAR algorithm with POLDER data over Africa. *IEEE Trans. Geosci. Remote Sens.* **2000**, *38*, 2402–2418. [[CrossRef](#)]

Disclaimer/Publisher’s Note: The statements, opinions and data contained in all publications are solely those of the individual author(s) and contributor(s) and not of MDPI and/or the editor(s). MDPI and/or the editor(s) disclaim responsibility for any injury to people or property resulting from any ideas, methods, instructions or products referred to in the content.